

DIS-Parity: Search for New Physics through Parity Violation in Deep Inelastic Electron Scattering

J.R. Arrington, K. Hafidi, R.J. Holt, H.E. Jackson,
D.H. Potterveld, P.E. Reimer, E. Schulte, X. Zheng
Argonne National Laboratory, Argonne, IL

Y. Kolomensky
University of California, Berkeley, CA 94720

R. Carr, B. Filippone, R. McKeown, M.J. Ramsey-Musolf
California Institute of Technology, Pasadena, CA 91125

E. Chudakov, D. Mack, R. Michaels
Jefferson Lab, Newport News VA 23606

S. Penttila
Los Alamos National Laboratory, Los Alamos, NM 87545

E.J. Beise
University of Maryland, College Park, MD 20742

R. Arnold, P.E. Bosted, R. Hicks, S.E. Rock
University of Massachusetts, Amherst, MA 01003

J. Erler
Universidad Nacional Autónoma de México, 04510 México D.F., México

S. Kuhn
Old Dominion University, Norfolk, Virginia 23529

P. Decowski
Smith College, Northampton, Massachusetts 01063

F.J. Decker, R. Erickson, T. Fieguth,
M. Olson, J.L. Turner, D. Walz, M. Woods
Stanford Linear Accelerator Center, Menlo Park, CA 94025

R. Homes, P.A. Souder
Syracuse University, Syracuse, NY 02130

D. Crabb, D. Day, P. McKee, O. Rondon, F.R. Wesselmann
University of Virginia, Charlottesville, VA 22901

D. Armstrong, T. Averett, K. Griffioen, M. Finn
College of William and Mary, Williamsburg, Virginia 23187

N. Akopov, A. Apyan, R. Avakian, A. Avetisian, K. Dallakyan
S. Darbinian, K. Ispirian, T. Navasardyan, S. Taroyan
Yerevan Physics Institute, Yerevan, Armenia

Abstract

We propose a precise measurement of the parity-violating interference between electromagnetic and weak coupling in deep-inelastic electron scattering from the deuteron (DIS-Parity). This reaction is sensitive to new physics beyond the electroweak Standard Model. The experiment will determine the Z -quark coupling to an equivalent precision in $\sin^2(\theta_W)$ of $\pm 0.0006(\text{stat.}) \pm 0.0006(\text{exp. sys.}) \pm 0.0004(\text{theory. sys.})$ (combined uncertainty of 0.0009 or 0.4%). This is a factor of 20 smaller than the previous experiment, and is smaller than the uncertainty of the NuTeV experiment, which has recently observed a 3σ deviation from the Standard Model value. We propose measurements near $Q^2 = 20 \text{ GeV}^2$ to minimize theoretical corrections. The use of the light isoscalar deuteron as a target greatly reduces nuclear corrections. We will be sensitive to new particles and interactions (in the semi-leptonic sector) which do not modify the properties of the Z boson, and hence would not have been observed in precision Z -pole measurements, such as Z' s, leptoquarks, and compositeness.

The experiment consists of scattering 36 and 39 GeV polarized electrons from a 100 cm long liquid deuterium target located in End Station A. The scattered electrons will be detected in two identical large solid angle magnetic spectrometers, each centered around a scattering angle of 12 degrees. Electrons will be identified and counted in an array of lead glass blocks. Pions will be identified and rejected by an additional detector array. The beam polarization will be measured using the Compton polarimeter adapted from SLD. We request a total of 5×10^8 beam pulses for checkout, calibration, and production running.

1 Introduction

There is a strong belief in the physics community that the Standard Model of particles and interactions is incomplete. A very large effort is going into direct searches for new physics with the upgraded Tevatron, the LHC, and plans for a Linear Collider (LC). Direct searches are complemented by precision electro-weak experiments that search for the indirect effects of new physics by comparison with expectations calculable in the Standard Model.

The effective Lagrangian describing parity violating e -hadron interactions is defined with couplings C_{ij} , which in the Standard Model are products of g_A and g_V couplings of the Z to the electron and to the quarks. In the Standard Model the C_{ij} are related to other electro-weak couplings of ν -hadron interactions (ϵ_L and ϵ_R), $\nu-e$ and $e-e$ interactions, and the $e^+ + e^- \rightarrow Z$ (A_f and V_f), and all the couplings are expressed in terms of $\sin^2(\theta_W)$. In general, new physics can modify the various couplings for these interactions independently in sign and magnitude. To explore the full range of new physics possibilities it is important

to have precision measurements of all the electro-weak couplings to look for any pattern of deviation from the Standard Model.

The indirect searches for new physics include measurements of rare decays and precision measurements of electroweak observables. Measurements have been made in electron-positron annihilation at the Z -pole, and in a variety of observables at low momentum transfer, Q^2 . Z -pole measurements primarily set limits of the effects of new physics that couples to the Z and the electron. Low Q^2 semi-leptonic measurements provide complementary constraints on new physics that does not couple strongly to the Z (for example, many classes of Z' particles), or requires interactions with quarks to be observed (for example quark sub-structure, or leptoquarks). Indirect effects of new physics can be interpreted in precision electro-weak observables as coming from differences in the weak couplings from their Standard Model values.

Within the Standard Model at tree level, for each fermion relevant in low energy processes (electron, up quark, and down quark), there are two couplings, which can be described as left or right handed, or equivalently as vector (sum of left and right) and axial vector (difference of left and right). Thus there are effectively six coupling or weak charge parameters in precision electroweak measurements, which in the Standard Model are denoted as $g_V^e, g_A^e, g_V^u, g_A^u, g_V^d, g_A^d$ and are related to $\sin^2(\theta_W)$. The usual assumption is that the couplings are generation independent (so muon and electron couplings are the same, and s and c quarks have the same couplings as d and u). Parity (P) and charge (C) violating experiments measure products of weak charges, and each has a different sensitivity to new physics, depending on how the new physics affects the particular observable. For example, E158 at SLAC measures parity violation (PV) in the purely leptonic electron-electron scattering and thus measures only $g_V^e g_A^e$. Semi-leptonic processes such as DIS-Parity, atomic parity violation (APV), e -p elastic scattering, and e -A elastic scattering are sensitive to combinations of the electron-quark couplings $C_{1u} = g_A^e g_V^u, C_{1d} = g_A^e g_V^d, C_{2u} = g_V^e g_A^u$ and $C_{2d} = g_V^e g_A^d$, shown in Table 1.

Experiments can report the values of the particular couplings compared with the Standard Model, or express the results as a value of $\sin^2(\theta_W)$ obtained by assuming the Standard Model relation between couplings and $\sin^2(\theta_W)$. If different experiments obtain different values for $\sin^2(\theta_W)$, this is a signal that the assumed relation between the couplings is wrong. The present outstanding example is the 3-sigma difference for $\sin^2(\theta_W)$ between the NuTeV value and the world average (mostly from Z -pole variables). Another example which may hint at new physics at the Z -pole is that A_e , a measure of the purely leptonic Zee vertex, gives different results for $\sin^2(\theta_W)$ than $A_{FB} \propto A_e A_f$ which includes the quark vertex. It is also possible that these variations in $\sin^2(\theta_W)$ from the Standard Model predictions are due to unaccounted for systematic errors in the measurements. Several measurements with unique experimental errors are required to sort out the differences.

The best sensitivity to C_{iq} at present comes from APV, which essentially is a measure of $C_{1u} + 1.1C_{1d}$. When combined with a planned high precision measurement of ep elastic scattering (QWeak at JLab), which essentially measures $-(2C_{1u} + C_{1d})$, the vector quark couplings will be determined at the percent level, equivalent to new physics at the TeV scale, *if* the new physics couples to the quark *vector* current. What is missing is sensitivity

to the physics that couples to the *axial-vector* quark current. Existing experiments (parity violation in e -D quasi-elastic, e -Be quasi-elastic, and e -D DIS, and charge asymmetry in muon DIS), provide only very weak limits (equivalent to approximately 100% errors on g_A^q). We propose to improve the experimental uncertainty in parity violating e -D DIS (DIS-Parity) by more than an order of magnitude, with a corresponding improvement in the sensitivity to new physics revealed by the axial quark current. This will also make a modest improvement in the sensitivity to the vector quark current. DIS-Parity is essentially proportional to $C_{1m} + Y C_{2m}$, where Y is a kinematic factor between 0 and 1, $C_{1m} = 2C_{1u} - C_{1d}$ and $C_{2m} = 2C_{2u} - C_{2d}$. In a combined fit with ep elastic and APV, the opposite signs in the C_1 combination help pin down C_{1u} and C_{1d} individually. At high Y (as in this proposal) the contribution of the C_2 terms is much larger in DIS-Parity than in other high-precision experiments. Figure 1 illustrates the improvement that our proposal will bring to the determination of C_{2m} , with and without the assumption that C_{1m} is determined from APV and ep elastic.

Improved knowledge of C_{2m} will have the added benefit of helping to pin down the poorly known product of electron (or muon) axial and quark axial charges, denoted as $C_{3u} = g_A^e g_A^u$ and $C_{3d} = g_A^e g_A^d$. A CERN experiment [1] measured the ratio of deep-inelastic cross section for positive and negative muons that is sensitive to the combination $C_{3m} + P_\mu C_{2m}$, where $C_{3m} = 2C_{3u} - C_{3d}$ and P_μ is the muon polarization (See Table 1). Our improved measurement of C_{2m} will allow a more precise extraction of the C_{3m} from the CERN data.

The bottom line is that DIS-Parity will provide a precise measurement of electroweak couplings at low Q^2 that are complementary to other existing or planned precision measurements. It will measure a unique combination of electron-quark couplings, that, together with the other precision experiments, will yield strong constraints on the possible deviations from the Standard Model predictions.

1.1 Brief History of Precision Measurements

The classic 1978-1979 SLAC DIS-Parity measurements [2] were pivotal in establishing the Weinberg-Salam electro-weak part of the Standard Model, which could primarily be distinguished from other models through the predicted small ratio of C_{2m}/C_{1m} and the overall predicted magnitude of the asymmetry. Assuming the Weinberg-Salam model, the extracted Z boson weak mixing angle was $\sin^2(\theta_W) = 0.222 \pm 0.018$ with a relative uncertainty of approximately 8%. The experiment consisted of scattering longitudinally polarized electrons from unpolarized liquid deuterium or hydrogen targets, and detecting the scattered electrons at 4 degrees in a momentum-analyzing spectrometer system. The 4-momentum transferred (Q^2) was relatively low, averaging 1.5 GeV². The interference between single photon and single Z exchange to the struck quark in the target resulted in an asymmetry between cross sections measured with the two beam helicities.

Since then, the SLD at SLAC and the four LEP experiments at CERN have provided a wealth of precision electro-weak data [3] at the Z pole (corresponding to $Q^2 = 8315$ GeV²). Combined with measurements of the W and top quark masses from the Tevatron, the consistency of $\sin^2(\theta_W)$ extracted from the various measurements has placed stringent

Table 1: Observables sensitive to the P or C violating coefficients C_{iq} . The errors are the combined (in quadrature) statistical, systematic and theoretical uncertainties. The first two lines result from a fit to 11 different kinematic points (a 5% uncertainty in the polarization was common to all points) and have a -92.7% correlation. The two CERN entries are for muon beam energies (polarizations) of 120 GeV (66%) and 200 GeV (81%), respectively. Assuming 100% correlated systematic errors yields a correlation of 17.4% between them. The second line (SLAC) contains a 31.6% correction to account for sea quarks, while the corresponding correction is 7.5% for CERN.

beam	process	$\overline{Q^2}$ [GeV ²]	combination	result/status	SM
SLAC	e^- D DIS	1.39	$2C_{1u} - C_{1d}$	-0.90 ± 0.17	-0.7185
SLAC	e^- D DIS	1.39	$2C_{2u} - C_{2d}$	$+0.62 \pm 0.81$	-0.0983
CERN	μ^\pm C DIS	34	$0.66(2C_{2u} - C_{2d}) +$ $2C_{3u} - C_{3d}$	$+1.80 \pm 0.83$	$+1.4351$
CERN	μ^\pm C DIS	66	$0.81(2C_{2u} - C_{2d}) +$ $2C_{3u} - C_{3d}$	$+1.53 \pm 0.45$	$+1.4204$
Mainz	e^- Be QE	0.20	$2.68C_{1u} - 0.64C_{1d} +$ $2.16C_{2u} - 2.00C_{2d}$	-0.94 ± 0.21	-0.8544
Bates	e^- C elastic	0.0225	$C_{1u} + C_{1d}$	0.138 ± 0.034	$+0.1528$
Bates	e^- D QE	0.1	$C_{2u} - C_{2d}$	0.015 ± 0.042	-0.0624
JLAB	e^-p elastic	0.03	$-(2C_{1u} + C_{1d})$	approved	$+0.0357$
SLAC	e^- D DIS	20	$2C_{1u} - C_{1d}$ $+Y(2C_{2u} - C_{2d})$	this proposal	-0.7185 $-Y0.0983$
SLAC	e^\pm D DIS	20	$2C_{3u} - C_{3d}$	future proposal (?)	$+1.5000$
—	^{133}Cs APV	0	$-376C_{1u} - 422C_{1d}$	-72.69 ± 0.48	-73.16
—	^{205}Tl APV	0	$-572C_{1u} - 658C_{1d}$	-116.6 ± 3.7	-116.8

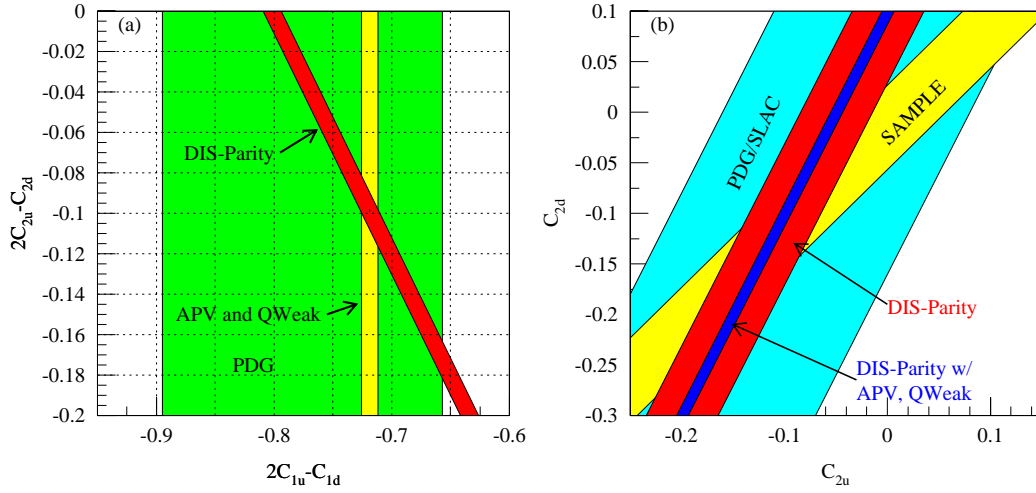


Figure 1: a) The area labeled PDG shows the present knowledge of C_{1m} and C_{2m} . The indicated band shows the sensitivity of this proposal, while the yellow band shows the combined sensitivity of existing APV and planned e - p elastic (QWeak at JLab) experiments. b) The present knowledge of C_{2d} and C_{2u} is shown by the band labeled PDG/SLAC from the experiment by C. Prescott et al [2]. The band labeled SAMPLE is from ed and ep at MIT-Bates. The indicated band shows the improvement from the present proposal alone, while the narrower band shows the improvement when APV and QWeak are used to constrain the contributions of C_{1u} and C_{1d} .

constraints on new physics [3, 4, 5]. The average of all existing measurements gives the remarkably precise value $\sin^2(\theta_W) = 0.23113 \pm 0.00015$ [3] at the Z mass in the $\overline{\text{MS}}$ scheme. However, the $\chi^2/\text{d.f.}$ for agreement of the precision measurements selected by the LEP Electro Weak Working Group is poor [5]. In particular, there is 3 standard deviation (3σ) discrepancy between leptonic and hadronic Z pole measurements. The forward-backward b asymmetry has the largest influence (pull) on the poor $\chi^2/\text{d.f.}$ of any of the measurements. All of this strongly hints at the possibility of new physics [4, 5], and motivates the need for additional precision measurements.

Since the new physics may couple relatively weakly to the Z , and because the Z propagator amplitude on resonance is purely imaginary and so new physics enters mainly through radiative corrections rather than direct interference, it has been long recognized that measurements away from the Z -pole are crucial. The NuTeV experiment [6] has measured neutrino-quark scattering at $Q^2 \approx 20 \text{ GeV}^2$ and has extracted $\sin^2(\theta_w)^{\text{on-shell}} = 0.2277 \pm 0.0016$, 3σ away from the expected value (see Fig. 2). This may be an indication of new physics [7]. On the other hand, conventional explanations related to the use of a heavy nucleus with a significant neutron excess (iron) for the target have also been put forward [8, 7]. The results for $\sin^2(\theta_W)$ at very low Q^2 have been obtained from Atomic Parity Violation (APV) on a variety of nuclei. This process is also sensitive to the electron-quark couplings. The interpretation has varied significantly over the past years, as large and difficult-to-calculate theoretical corrections have evolved. The most recent analysis of results from isotopes of Cesium [9], shown in Fig. 2, are in reasonable agreement with the Standard Model, although past analyses have shown up to 2σ discrepancies as recently as a year ago.

An ongoing experiment at SLAC, E158 [10], aims to measure an effective value of $\sin^2(\theta_W)$ at $Q^2 = 0.03 \text{ GeV}^2$ in the electron sector using Møller scattering with a precision somewhat better than the NuTeV experiment. The asymmetry in this experiment is proportional to $[1/4 - \sin^2(\theta_W)]$, and benefits from increased sensitivity due to the electro-weak running of $\sin^2(\theta_W)$, which becomes closer to 0.25 at low Q^2 (see curve from Ref [11] on Fig. 2).

1.2 Future Experiments and this Proposal

Clearly, additional measurements away from the Z -pole in the hadron sector are called for to clarify the experimental situation, and either provide evidence for, or set limits on, the existence of new physics. Experiments on proton or deuteron targets are essential to minimize nuclear/atomic corrections. An approved experiment at Jefferson Lab (E02-020/QWeak) [12], plans to measure $\sin^2(\theta_W)$ with good precision using ep elastic scattering at $Q^2 \approx 0.03 \text{ GeV}^2$. The present DIS-Parity proposal will provide timely and complementary measurements on an orthogonal combination of weak charges.

The previous SLAC DIS-parity results are no longer relevant for precision electroweak constraints on the Standard Model. Many factors now make it possible to re-do the SLAC experiment with the order-of-magnitude improvement in precision and average Q^2 to make it relevant and competitive. These factors include:

- higher beam energy

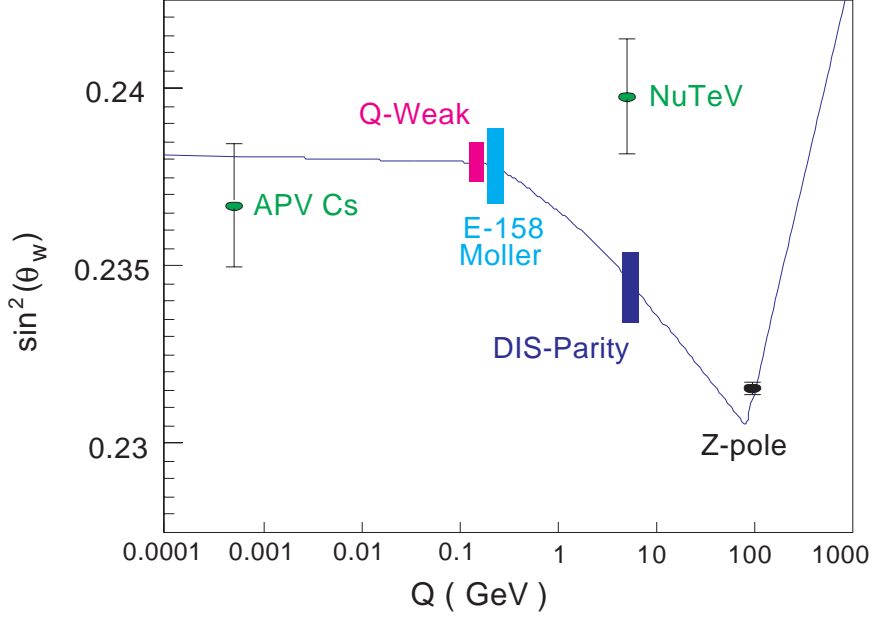


Figure 2: Predicted running of $\sin^2(\theta_W)$ as a function of Q^2 in the $\overline{\text{MS}}$ scheme from [11] compared with existing data from Atomic Parity Violation (APV) [9], NuTeV [6], and Z-pole measurements [3], and anticipated errors from SLAC E158 [10], Jefferson Lab QWeak [12], and the present proposal (DIS Parity).

- higher beam current
- much higher beam polarization
- larger spectrometer acceptance
- longer high power cryogenic targets
- much improved control of helicity-correlated beam parameters
- better beam polarization measurements
- better knowledge of parton distribution functions
- better understanding of higher twist in QCD

Most of these improvements have been solidly established by the ongoing E158 experiment. The improvements will enable a measurement with a combined statistical and systematic uncertainty on $\sin^2(\theta_W)$ of about 0.0009, comparable to the currently expected E158 uncertainty of 0.0010 to 0.0016, and about 60% of the NuTeV uncertainty. While the JLab QWeak experiment projects a smaller error than E158 and DIS Parity, it measures an orthogonal combination of quark couplings, making it complementary rather than competitive. We are confident that the DIS-Parity experiment we are proposing could be built, run,

and analyzed within three to four years of approval, given a sufficient level of support It will provide the a theoretically clean high precision semi-leptonic measurement away from the Z -pole.

The combined results from the new E158, QWeak and DIS-Parity experiments will greatly increase the sensitivity to new physics. With their different sensitivities to lepton and quark couplings, they could establish properties of new particles or interactions that might be observed directly at the Tevatron or LHC.

SLAC is the only place where this experiment can be carried out in the foreseeable future. While DIS-parity could also be measured at an upgraded (12 GeV) Jefferson Lab, the time scale is of order ten years away, and the limited Q^2 reach would result in significantly larger systematic errors from corrections such as dynamic higher twist. To help guide the direct searches, it is essential to have as much precision data as possible before the LHC accumulates significant statistics. The present proposal is both timely and cost-effective.

2 Definitions

The experiment consists of measuring the asymmetry between scattering left- and right-handed polarized electrons from unpolarized nucleons. In the Standard Model, the asymmetry arises from the interference between photon and Z exchange diagrams, and is given by [13]

$$A = \frac{\sigma_R - \sigma_L}{\sigma_R + \sigma_L} = -\frac{2Q^2}{M_Z^2} \frac{\sum f_i(x)(Q_i^{\gamma}/e)[g_A^e g_V^i + Y g_V^e g_A^i]}{\sum f_i(x)(Q_i^{\gamma})^2}, \quad (1)$$

where $f_i(x)$ are the quark distribution functions for a quark of type i , the g 's are the electroweak axial and vector charges, $Q^2 = -q^2$ is the four-momentum transfer squared ($Q^2 > 0$ for our kinematics), M_Z is the mass of the Z boson, and

$$Y = \frac{1 - (1 - y)^2}{1 + (1 - y)^2 - y^2 R / (1 + R)} \quad (2)$$

where $y = \nu/E$, $\nu = E - E'$ is the energy lost by an incident electron of energy E scattering to an electron of energy E' , and the factor $R = \sigma_L/\sigma_T$ takes into account [14] the longitudinal contributions to both Z and photon exchange. Performing the sums and re-writing M_Z in terms of the α and G_F coupling constants, for a proton target we obtain

$$A_p = \frac{3G_F Q^2}{\pi\alpha 2\sqrt{2}} \frac{2C_{1u}[u(x) + c(x)] - C_{1d}[d(x) + s(x)] + Y[2C_{2u}u_v(x) - C_{2d}d_v(x)]}{4u(x) + d(x) + s(x) + 4c(x)}. \quad (3)$$

where the products of weak charges in the Standard Model at tree level are given by:

$$\begin{aligned} C_{1u} &= g_A^e g_V^u \\ C_{1d} &= g_A^e g_V^d \\ C_{2u} &= g_V^e g_A^u \\ C_{2d} &= g_V^e g_A^d. \end{aligned} \quad (4)$$

When Standard Model electroweak radiative corrections are included the C_{ij} become [15]

$$\begin{aligned}
C_{1u} &= \rho' \left(-\frac{1}{2} + \frac{4}{3} \kappa' \sin^2(\theta_W) \right) + \lambda_{1u} \approx -0.1886 \\
C_{1d} &= \rho' \left(\frac{1}{2} - \frac{2}{3} \kappa' \sin^2(\theta_W) \right) + \lambda_{1d} \approx 0.3414 \\
C_{2u} &= \rho \left(-\frac{1}{2} + 2\kappa \sin^2(\theta_W) \right) + \lambda_{2u} \approx -0.0359 \\
C_{2d} &= \rho \left(\frac{1}{2} - 2\kappa \sin^2(\theta_W) \right) + \lambda_{2d} \approx 0.0265.
\end{aligned} \tag{5}$$

In the limit of no electroweak radiative correction $\rho = \rho' = \kappa = \kappa' = 1$ and $\lambda_{1u} = \lambda_{1d} = \lambda_{2u} = \lambda_{2d} = 0$.

We have assumed that the u , d , s , and $c(x)$ quark parton distribution functions (PDFs) of the proton can be described in terms of valence (v) and sea (s) contributions as

$$\begin{aligned}
u(x) &= u_v(x) + u_s(x) + \bar{u}_s(x) \\
d(x) &= d_v(x) + d_s(x) + \bar{d}_s(x) \\
s(x) &= s_s(x) + \bar{s}_s(x) \\
c(x) &= c_s(x) + \bar{c}_s(x)
\end{aligned} \tag{6}$$

The quark distribution functions depend mainly on the Bjorken scaling variable $x = Q^2/2M\nu$ (where M is the nucleon mass), but also evolve slowly with Q^2 due to QCD and finite mass corrections. While not shown explicitly, all quantities involving PDFs are functions of both x and Q^2 .

In the case of the deuteron, the assumption of isospin symmetry is generally made (i.e. all u and d distributions interchanged for the proton and neutron, but the s and c distributions remain unchanged), and in this case the asymmetry can be written as

$$A_d = \frac{3G_F Q^2}{\pi\alpha 2\sqrt{2}} \frac{2C_{1u}[1 + R_c(x)] - C_{1d}[1 + R_s(x)] + Y(2C_{2u} - C_{2d})R_v}{5 + R_s(x) + 4R_c(x)} \tag{7}$$

where

$$\begin{aligned}
R_c(x) &= \frac{2c(x)}{u(x) + d(x)} \\
R_s(x) &= \frac{2s(x)}{u(x) + d(x)} \\
R_v(x) &= \frac{u_v(x) + d_v(x)}{u(x) + d(x)}.
\end{aligned} \tag{8}$$

At sufficiently high x , the relative importance of sea quark contributions approaches zero, and $R_v \rightarrow 1$, $R_c \rightarrow 0$, and $R_s \rightarrow 0$. This is the ideal situation for a determination of $\sin^2(\theta_W)$, because A_d is insensitive to parton distribution functions.

Numerically, A_d is approximately given using Eq. 5 and Eq. 7 by

$$A_d = -10^{-4} Q^2 \frac{[0.78 + 0.41R_c(x) + 0.37R_s(x) + 0.10YR_v(x)]}{[1 + 0.2R_s(x) + 0.8R_c(x)]}, \quad (9)$$

where Q^2 is in units of GeV^2 . In the valence quark region ($R_c = R_s = 0$, $R_v = 1$), Eq. 7 becomes

$$A_d = -10^{-4} Q^2 [1.62(1 + Y) - \sin^2(\theta_W)(3.60 + 6.47Y)]. \quad (10)$$

Taking the derivatives, we find

$$\frac{d \sin^2(\theta_W)}{\sin^2(\theta_W)} \approx \frac{dA_d}{A_d} \frac{0.91 + 0.12Y}{1 + 1.8Y}. \quad (11)$$

Measurements at large Y clearly give the best sensitivity to $\sin^2(\theta_W)$. In the limit $Y \rightarrow 1$, a desired relative uncertainty of 0.4% on $\sin^2(\theta_W)$ requires a relative uncertainty on A_d of 1.1%.

The experimental asymmetry is diluted by the beam polarization P_e , so that

$$A_{exp} = \frac{N_+ - N_-}{N_+ + N_-} = P_e A,$$

where N_+ and N_- are the number of scattered electrons detected from + and - beam helicities respectively. The statistical uncertainty is given by

$$\delta A = \frac{1}{P_e \sqrt{N_+ + N_-}}.$$

For Q^2 in the 20 GeV^2 range, on the order of 5×10^9 electrons must be detected to achieve a 1% uncertainty in the physics asymmetry.

3 Physics Discovery Potential

3.1 Advantages of DIS-Parity

Precision measurement of the asymmetry in polarized deep inelastic electron scattering offers a unique window into some of the key outstanding issues in our understanding of the structure of matter. There are three main reasons for this. The first is that the asymmetry, which arises from the parity-violating nature of the Z coupling to electrons and quarks, is made visible by the interference between exchange of γ and Z . This exposes the amplitude of the effective electron-quark interaction via Z exchange and makes it possible to look for other small couplings to new layers of matter that would be too small to see in the squared amplitude of a direct cross section. Examples of new physics that might be exposed could arise from exchange of higher mass Z' bosons or from the compositeness of quarks and electrons.

The second advantage of DIS parity measurements is that they involve exchange of Z between electrons and quarks and thus will be sensitive to physics that might not be seen in purely leptonic observables, such as the precision A_{LR} at SLC and A_{FB}^l at LEP. There is currently a 3σ disagreement [4] between purely leptonic observables and semi-leptonic observables at the Z pole from SLC and LEP. The recent NuTeV [6] result at low Q^2 from ratios of neutrino cross sections involving a particular set of semi-leptonic charged and neutral current reactions is 3σ from the Standard Model prediction. A precision measurement of DIS parity will add a theoretically clean semi-leptonic observable to the world data below the Z pole at Q^2 similar to NuTeV, complementary to the purely leptonic measurement of Møller scattering by E158, and will provide timely and essential clues as to the source of these discrepancies.

The third advantage of a precision DIS parity measurements is that they examine the Z coupling to electrons and quarks at low Q^2 far below the Z pole. There are several reasons why this is important. The first is that in the Standard Model the electroweak mixing angle $\sin^2(\theta_W)$ is expected to evolve with Q^2 in a well-determined manner for a given renormalization scheme. It is very important to confirm the Q^2 evolution of the electroweak couplings. Several other precision measurements of $\sin^2(\theta_W)$ at low Q from existing experiments (APV [9], NuTeV [6]), experiments in progress (Møller-E158 [10]), and planned experiments (QWeak at JLAB [12] and the present DIS-Parity proposal)) are shown in Fig. 2 compared with the Standard Model expectation [11] in the $\overline{\text{MS}}$ scheme. The current data from APV and NuTeV give an inconsistent picture of the running of $\sin^2(\theta_W)$ with APV close to 1.0σ below and NuTeV 3σ above the Standard Model. E158 will test the running of $\sin^2(\theta_W)$ in a purely leptonic interaction. Each of the low Q^2 semi-leptonic experiments is sensitive to a particular combination of quark and lepton couplings (see Table 1) and has unique issues with systematic errors. A measurement of DIS parity with its particular combination of couplings and completely different systematic errors will significantly strengthen the constraints to help sort out the running of $\sin^2(\theta_W)$ from possible signals of new physics. The other main advantage of measurements at low Q^2 is that they may expose new physics that is either invisible in principle at the Z pole or not present at tree level and would make very small effects in the present world data dominated by Z pole and W observables. Examples of such effects would be from compositeness of quarks and leptons or from extra higher mass Z' that have small or no mixing with the Z .

3.2 Interpretability

The clear interpretability of our proposed DIS parity experiment makes it an attractive method for probing new physics. The measurement we propose at $x > 0.3$ and $Q^2 \approx 20$ GeV² on deuterium can be cleanly interpreted as the incoherent sum of scattering from the valence quarks of an isoscalar target. It is important for any clean probe of new physics that it not be compromised by uncertainties from hadronic structure or corrections for experimental effects that could cloud the interpretation. The main issues to be addressed are contributions from the sea quarks, coherent scattering from higher twist terms, uncertainties from electromagnetic and Standard Model electroweak radiative corrections, and the

small charge symmetry breaking between the proton and neutron quark distributions. In the sections below we explain in more detail how DIS scattering from the quarks can be cleanly extracted. Briefly, the kinematics are chosen at $x > 0.3$ to be far above the sea quarks at low x , and the $Q^2 \approx 20 \text{ GeV}^2$ ensures that the higher twist contributions are strongly suppressed. The electromagnetic radiative corrections are well understood from our previous work in DIS scattering. The electroweak radiative corrections are not large and can be reliably calculated in perturbation theory. The charge symmetry breaking effects which may cause up and down quark distributions in the proton and neutron to be unequal ($u_p \neq d_n$) are expected to be very small.

The results of our proposed DIS parity measurement can be cleanly interpreted in terms of the low energy effective electron-quark couplings C_{1u} , C_{1d} , C_{2u} , and C_{2d} . The C_{1i} arise from the interference of axial Z -electron coupling and vector Z -quark coupling ($g_A^e g_V^q$) while the C_{2i} are the opposite ($g_V^e g_A^q$). The C_{1i} couplings also appear in the weak charges Q_W , the coherent sum of the quark weak charges of the Cesium nucleus measured in APV and the proton measured in ep elastic. APV measures $Q_W(Cs) = -376C_{1u} - 422C_{1d}$ while ep elastic measures $Q_W(p) = -2(2C_{1u} + C_{1d})$ with no contributions from C_{2q} . The C_{1q} and C_{2q} couplings are most sensitive to extensions of the Standard Model from “direct” new physics at tree level which can be approximated by new four-fermion contact interactions [16]. The sensitivities to “oblique” new physics that affects the Z propagator or from loop and vertex terms in electroweak radiative corrections are small. The small size of the electroweak radiative corrections makes C_{1q} and C_{2q} insensitive to the mass of the Higgs boson and the top quark. Therefore we look for new physics that might appear from direct exchange of new particles or modification of the effective couplings from compositeness or presence of nonstandard fermions.

The asymmetry A_d at large values of the kinematic parameter Y gets contributions from both the C_{1q} and C_{2q} couplings from a term with $(2C_{1u} - C_{1d})$ and a term with $Y(2C_{2u} - C_{2d})$. The C_{2i} are small because $2\sin^2(\theta_W)$ is numerically close to $\frac{1}{2}$, so the term with C_{1q} makes the largest contribution to A_d . We see from Eq. 11 that the overall uncertainty in $\sin^2(\theta_W)$ extracted from DIS parity for a given uncertainty on A_d is reduced by a factor of roughly 0.4 when $Y = 0.8$ compared to $Y = 0$. Measurements at large Y give the best sensitivity to new physics when modifications to the effective $(2C_{1u} - C_{1d})$ and $(2C_{2u} - C_{2d})$ couplings are of the same sign, which is generally the case. Maximizing the sensitivity to $(2C_{2u} - C_{2d})$ also provides the best complementarity with other experiments, such as APV and QWeak.

3.3 How New Physics Enters into A_d

Detailed examination of the sensitivity of electroweak observables to possible extensions to the Standard Model are presented in Ref. [17] and updated [15] in the recent Review of Particle Data. A recent examination of the impact of possible new four-fermion contact interactions on low-energy parity-violating observables is presented in Ref. [18]. One way to characterize possible new physics that might appear, in analogy to the way the Fermi theory of beta decay is the low energy approximation of the weak interaction via W exchange, is

in terms of a generic four-fermion Lagrangian of the form:

$$\mathcal{L}_{NEW} = \frac{4\pi\kappa^2}{\Lambda^2} \sum_{q,i,j} h_{ij}^q \bar{e}_i \gamma_\mu e_i \bar{q}_j \gamma^\mu q_j. \quad (12)$$

Here κ is the coupling strength of the new interaction, Λ is the characteristic mass of the new degree of freedom, and the h_{ij} are the helicity-dependent coupling parameters with i and j denoting the handedness of the given fermion. Each scenario for new physics gives a prescription for the range of κ , Λ , and h_{ij} that might be expected.

From this we already see a feature that gives a major advantage of the low-energy parity-violating experiments for probing the new physics. The size of any possible effect is proportional to the ratio κ/Λ , so low energy experiments simultaneously probe the coupling strength and the mass scale of the new physics. This is to be compared with searches for new physics by direct production at high energy, for example by Drell Yan production followed by decay into lepton pairs (e.g. μ^+, μ^-) at the Tevatron. That process is sensitive to the mass scale Λ but also to the branching ratio to lepton pairs and therefore has different sensitivity to the new physics compared to the low energy experiments. If new particles are discovered at the Tevatron or elsewhere by direct production at high energy, the mass of the new particles would be known, but the coupling strength would be difficult to determine as it is buried in the production cross section from some unknown reaction mechanism and summed over incident quark distributions. The low energy experiments could play a very important role in measuring, or setting limits on the style and size of the couplings of any new particles discovered at high mass.

Each low energy experiment is uniquely sensitive to different features of the possible couplings. Møller scattering, for example, only involves electrons, so it would not probe quark compositeness or leptoquarks, but it might sense electron compositeness. In some new physics scenarios, for example non-standard extra fermions or coupling to leptoquarks, the new physics could come in with different weighting in Q_W and DIS parity depending on the relative contribution of up and down quarks in the observables. If the new physics effectively modifies the coupling C_{1q} differently from the modification of C_{2q} , this would affect DIS-Parity and QWeak observables differently. Finally, the current 3σ deviation of NuTeV from the Standard Model occurs in reactions involving both neutral and charged weak currents, whereas the DIS parity and Q_W only involve neutral currents. Precision measurements of different low Q^2 observables in the different experiments, each with unique sensitivity and unique experimental uncertainties, offers the best chance to sort out or set limits on the type and strength of any new physics. Precision DIS parity can play an important role in this enterprise.

3.4 Models of New Physics

To illustrate the sensitivity of our proposed total measurement error of 0.0009 on $\sin^2(\theta_W)$ using DIS parity violation, we consider three possible sources of new physics: extra Z' bosons, electron and quark compositeness, and leptoquarks.

3.4.1 Extra Z' bosons

Extra Z' bosons are one of the best-motivated extensions of the Standard Model. They are present in most models in which the Standard Model is embedded into a unifying group, and they arise in some models with extra dimensions. Most models of string theory also predict extra $U(1)'$ symmetries and therefore possibly Z' s. In particular, in the context of SUSY, $U(1)'$ symmetry breaking may be triggered by SUSY breaking and the Z' mass would in this case be expected to be roughly at the electroweak scale, and could leave traces in low-energy precision measurements. The presence of Z' could show up as a change in the Z couplings due to mixing, direct Z' exchange, and a reduction in the Z mass from mixing. The size of any effects from extra Z' would be determined by the mass and couplings of the Z' and the mixing angle with the Z . Present data [19] place some limits on the existence of Z' . They have not been seen in direct searches at the Tevatron with lower mass bounds around 600 GeV. Tevatron Run II may extend the mass sensitivity to approximately 1 TeV. The existence of a Z' that mixes with the Z is strongly constrained by the LEP and SLC data, but a new Z' that does not mix with the Z is not ruled out and might show up at low Q^2 .

Extensions of the Standard Model invoking new Z' have been explored in detail by various authors [17, 18, 20] where explicit suggestions for the factors in Eq. 12 for the coupling strength κ , the helicity couplings h_{ij} for a Z' with mass $\Lambda^2 = M_{Z'}^2$, are used to estimate the effect on the C_{1i} and C_{2i} . The calculations show DIS parity to be most sensitive to Z' which are left-right symmetric where $SU(2)_L$ and $SU(2)_R$ couplings are identical. In that case our proposed measurement uncertainty of 0.0009 on $\sin^2(\theta_W)$, taking into account contributions from both C_{1i} and C_{2i} , will set limits on the existence of Z'_{LR} , even in the absence of $Z - Z'$ mixing, up to about 1.5 TeV.

3.4.2 Compositeness

Electron and quark compositeness could manifest itself as a four-fermion type interaction from the interchange of constituents as illustrated in Fig. 3. There are many invariant operators that can be constructed that satisfy $SU(3) \times SU(2) \times U(1)$ at low energies that bring in a new interaction at compositeness scale $\Lambda > M_Z$. It is conventional to write the lowest dimension contact interactions between electron and quark as

$$\mathcal{L}_{comp} = \sum_{q,i,j} \eta_{ij}^q \bar{e}_i \gamma_\mu e_i \bar{q}_j \gamma^\mu q_j. \quad (13)$$

where i, j indicates the fermion chiralities. For reactions on up and down quarks there are eight independent coefficients $\eta_{LL}^u, \eta_{LR}^u, \eta_{RL}^u, \eta_{RR}^u, \eta_{LL}^d, \eta_{LR}^d, \eta_{RL}^d, \eta_{RR}^d$ with dimensions $(\text{TeV})^{-2}$ which are conventionally expressed as $\eta_{ij}^q = \epsilon g^2 / \Lambda_{ij}^q$, where the coupling g is usually fixed at $g^2 = 4\pi$. The factor $\epsilon = \pm 1$ allows for either constructive or destructive interference with the Standard Model γ and Z exchange amplitudes, and Λ_{ij}^q represents the mass scale of the exchanged new particles with coupling $g^2 = 4\pi$. The parity violating observables in DIS Parity or APV pick out certain linear combinations of η_{ij} coefficients that give the

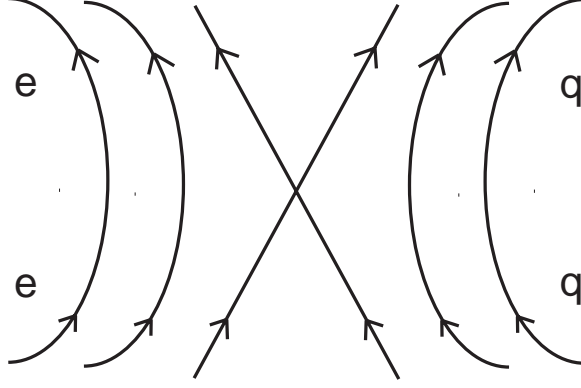


Figure 3: Constituent interchange diagram, leading to 4-Fermi eq interaction.

$(A^e \times V^q)$ and $(V^e \times A^q)$ structure in the C_1 and C_2 coefficients. The compositeness contact interaction would modify the C_{1q} and C_{2q} by an amount scaled to the standard weak coupling as

$$\begin{aligned}\Delta C_{1q} &= \frac{1}{2\sqrt{2}G_F}[-\eta_{LL}^q + \eta_{RR}^q - \eta_{LR}^q + \eta_{RL}^q] \\ \Delta C_{2q} &= \frac{1}{2\sqrt{2}G_F}[-\eta_{LL}^q + \eta_{RR}^q + \eta_{LR}^q - \eta_{RL}^q]\end{aligned}\quad (14)$$

Such four-fermion operators do not affect M_W or M_Z and their contributions to Z -pole observables are second order. A direct search experiment would have to reach energies near the mass scale Λ to be sensitive.

Several types of current data can be used to look for fermion-quark compositeness. A recent review [16] fit the Standard Model plus four-fermion contact interaction to the world data (DIS at HERA, Drell-Yan cross sections from the Tevatron, hadron production at LEP, atomic parity violation in Cs (APV), polarized electron scattering from nuclei at SLAC, Mainz, Bates, neutrino-nucleon scattering from CCFR) and extracted limits on the compositeness mass scale for the various chirality couplings. DIS-Parity is sensitive to couplings Λ_{LL} and Λ_{RR} but not to Λ_{LR} and Λ_{RL} which nearly cancel in the combinations of C_1 and C_2 that are measured. The best limits for the Λ_{LL} and Λ_{RR} from the world data are obtained from the APV data, which require large and difficult-to-calculate theoretical corrections that have changed significantly in recent evaluations. Plotted in Figure 4 are the compositeness mass limits at the 95% confidence level from Ref. [16] for the the case $\Lambda_{LL}^u = \Lambda_{LL}^d$ from the various world data sets compared to the 2σ limit $\Lambda > 6.9$ TeV expected from this proposed DIS-Parity measurement. The limits are given assuming only the η_{LL}^q coupling chirality is present for both up and down quarks and all the rest are zero, and for the case of constructive interference ($\epsilon = +1$). The DIS-Parity result will give stronger limits than all but the APV result. Similar limits for $\Lambda_{RR}^u = \Lambda_{RR}^d$ will be determined in DIS Parity. Given that the theoretical uncertainty for DIS-Parity is expected to be small, this new measurement will be the most powerful clean measurement of electron-quark compositeness.

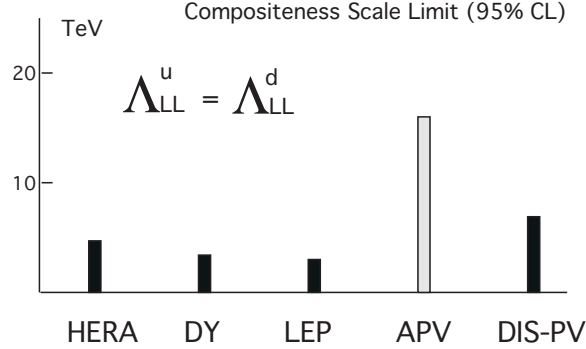


Figure 4: Sensitivity to electron-quark compositeness mass scale from a fit to current world data [16] and the present proposal. Values are for assumed Left-Left contact interactions between the electron and the up and down quarks, taken one at a time with other couplings set to zero, and for the case of constructive interference of the new physics with the SM amplitudes. Best estimate for world values are from Table 4, Ref. [16].

3.4.3 Leptoquarks

Finally we consider the sensitivity of DIS-Parity to leptoquarks. Leptoquarks are hypothetical bosons which couple to a lepton and a quark via a Yukawa coupling (λ), such that leptoquarks could be singly produced in lepton-quark interactions. Leptoquarks are usually assumed to be generation diagonal, and they occur in various species that are characterized by the chirality of the lepton-quark coupling, the spin $J = 0$ (scalar), or 1 (vector), the weak isospin, and the fermion number $F = 3B + L = 0$ or 2. We use the analysis in Ref. [18] where the possible parity violating effects from interactions on first generation quarks of the type $eq \rightarrow LQ \rightarrow eq$ for both scalar and vector leptoquarks are examined. In terms of the parameters in Eq. 12

$$\begin{aligned} \Lambda^2 &= M_{LQ}^2 \\ \kappa^2 &= \lambda_{S(V)}^2/16\pi \end{aligned} \tag{15}$$

and $h_S^q = 1/2$ ($h_V^q = -1$) for scalar (vector) leptoquark interactions. Assuming for simplicity creation of a scalar leptoquark from interactions with u quarks, but not d quarks, the 2σ limits from DIS-Parity will be approximately

$$\lambda_S \leq 0.025(M_{LQ}/100 \text{ GeV}) \tag{16}$$

The present limits for various leptoquarks from data at HERA, L3 and D0 are collected and displayed in Ref. [21]. The present limits in the coupling/mass plane for the scalar leptoquark S_0^L (weak isospin = 0, couples to left handed fermion) from Ref. [21] together with the limit from DIS-Parity are shown in Fig. 5. Assuming the mass limit of $M_{LQ} = 200$ GeV from D0, which is not sensitive to λ , then a measurement of A_d will put a 95 % confidence limit of approximately 0.050 on λ_S . Or assuming $\kappa^2 = \alpha_{EM}$, DIS-Parity would put mass bounds on the scalar LQ at $M_{LQ} > 2.4$ TeV. This limit would be better than the

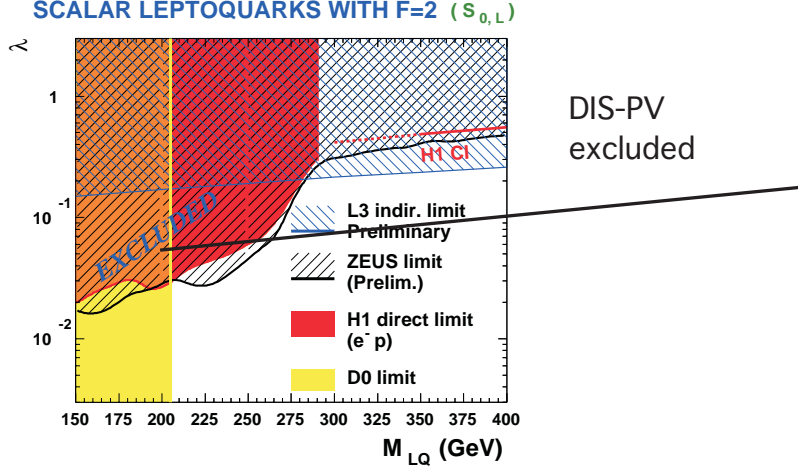


Figure 5: Limits on S_0^L leptoquarks in the (M_{LQ}, λ) plane. The excluded region lies above the curves for H1, L3, and ZEUS and to the left of the line for D0 (from Fig 1 in Ref. [21]). The λ in this plot is $2\lambda_S$ in Eq 16. The additional limit obtained from DIS-Parity is above the dark solid line.

present 2σ limit of $M_{LQ} > 1.5$ TeV from APV in an experiment with completely different and relatively smaller systematic errors. The estimated reach of Tevatron Run II is about 300 GeV.

DIS-Parity will provide complementary information to the direct search experiments and will significantly extend the limits on the existence of leptoquarks beyond those currently set in direct searches.

3.5 Other Physics

The experimental setup we propose could be used with only minor changes for other physics investigations. Changing the target from LD2 to LH2 would allow the study of the d/u quark ratio in the valence region. Presently d/u mainly comes from comparing spin-averaged cross sections on protons and neutrons in deuterium targets. The interpretation at high x is complicated by the uncertainty in deuteron structure, and possible charge symmetry violation between the proton and neutron. A parity-violating measurement on a hydrogen target would be free of both of these problems, and adequate statistical accuracy could be

obtained with the present apparatus in a reasonable amount of time.

Better measurements of the strange and charm quark distributions could be obtained with no changes to the proposed apparatus, simply by lowering the momentum of the spectrometer.

Measurements could also be made on carbon or heavier nuclei. Nuclear corrections would be similar to those for NuTeV, and could provide a valuable constraints on the interpretation of this experiment.

Finally, we could improve on the CERN measurements [1] of the ratio of spin-averaged cross sections for positive and negative lepton beams with basically no change to the proposed equipment, other than the addition of a forward luminosity monitor and possibly improved instrumentation on the target for high precision temperature and pressure measurements.

4 Experimental Plan

4.1 Kinematics

Several parameters dictate the experimental setup needed to achieve the physics goals outlined above. To keep higher twist corrections to A_d below 0.2%, we require $Q^2 > 10 \text{ GeV}^2$ and the invariant mass of the final hadrons $W > 5 \text{ GeV}$. We also require $x > 0.3$ so that the uncertainty due to parton distribution functions is below 0.2%. To maximize the sensitivity to new physics affecting C_2 , we would like Y as large as possible. We further require the ratio of scattered to incident electron energy $E'/E > 0.2$ to keep the uncertainty on electromagnetic radiative corrections below 0.3%, and to avoid high rates of pion and pair-symmetric backgrounds. Taken together, these requirements imply a beam energy of at least 25 GeV and an electron scattering angle of at least 10 degrees. To determine the effective average Q^2 of the measurements to better than 0.3%, we also require rates per SLAC beam spill that are low enough to allow counting of each electron, rather than the flux integration method used in the previous eD parity experiment and in E158. The counting mode allows backgrounds from pions, beam halo, soft photons, and electrons that scatter on the edges of apertures in the spectrometer to be rejected on an event by event basis, leaving a clean sample of well-identified electrons. On the other hand, the rates must be large enough to allow a 0.7% relative uncertainty on A_d in a reasonable number of spills, which we have chosen to be 4×10^8 (similar to the recent E154 and E155 experiments, and about half of the E158 experiment). Taking into account that the solid angle of a typical magnet spectrometer increases slowly with increasing angle and lower average momentum, the optimum beam energy is around 37 GeV, and the optimum spectrometer angle is 12 degrees. In practice, we will split the data taking between 35.60 and 38.84 GeV, which differ by π in $g - 2$ precession through the A-line. This provides a valuable check of helicity-correlated systematic errors in the beam parameters.

4.2 Electron Beam

A tremendous effort has recently gone in to achieving a low jitter, high current electron beam with very small helicity correlations in current, energy, position, and angle. This has allowed E158 to measure the asymmetry in Møller scattering with a systematic error due to beam parameters below 10^{-8} . The beam improvements include

- ESA DAQ control over source helicity feedbacks
- higher power and stability for the source laser
- new helicity-correlated position feedback at the source
- a new gradient-doped, strained lattice cathode that overcomes the charge limit effect
- new electronics for BPMs and toroids in the A-line and ESA
- new feedbacks in the Linac and A-line
- new energy compensation techniques to allow high-charge long-pulse operation with low energy spread
- introduction of a skew quad at the end of the A-line to reduce sensitivity to the vertical beam emittance and its fluctuations

No additional improvements to the electron beam are needed for the present proposal. Our requirements are much less stringent than for E158, due to the four orders of magnitude larger asymmetry. Since we can easily tolerate a factor of ten more beam jitter than E158, we propose to use a beam current of 9×10^{11} electrons/spill (a factor of 1.5 higher than used in E158 at 45 GeV). A recent test at 42 GeV demonstrated that this current is possible, and that beam fluctuations are small enough for the present proposal.

4.3 Compton Polarimeter

The purpose of the Compton polarimeter is to measure the longitudinal beam polarization with an accuracy of 0.3%. An accuracy of 0.5% has already been achieved in the SLD experiment with essentially the same apparatus, and some upgrades and improved procedures should allow a higher degree of accuracy. There is a strong interest from the LC community to demonstrate that an accuracy of 0.25% (or better) with such a polarimeter is possible, and the present proposal will provide a good test case due to the similarity in beam parameters to those of the LC. To allow continuous monitoring of the beam polarization, the apparatus will be located up-beam of the target, as shown in Fig. 6. We plan to re-use as much of the SLD apparatus as possible.

The apparatus consists of an analyzing magnet and nine threshold Cherenkov counters to detect electrons scattered from a high-powered laser beam. The physical layout is shown in Fig. 6. The primary electron beam is steered back onto the nominal beamline by two additional magnets. An additional detector is being considered to detect recoil photons, as

COMPTON POLARIMETER

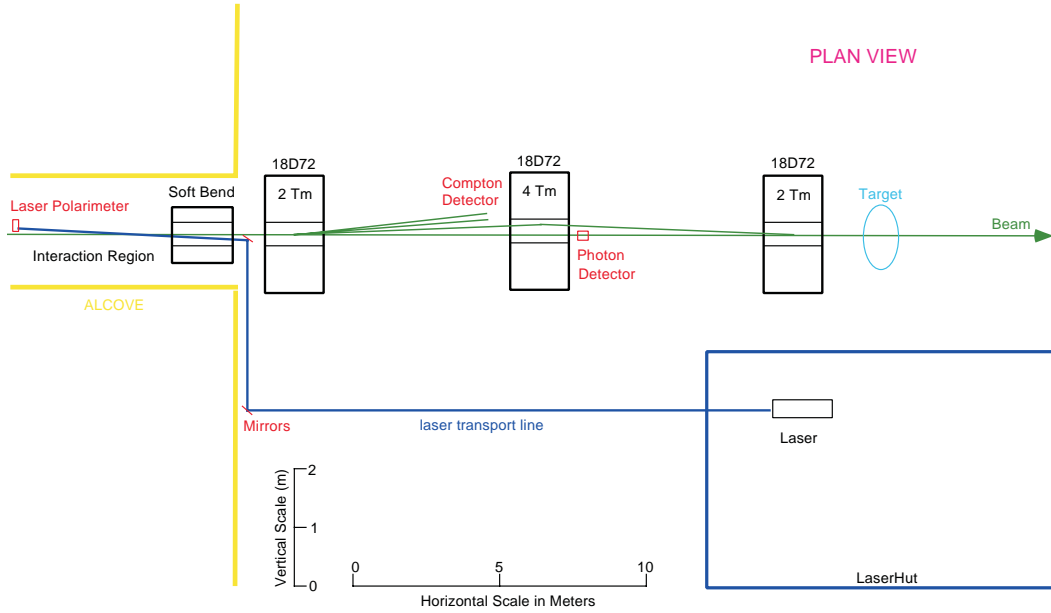


Figure 6: Schematic layout of the Compton Polarimeter in the front part of End Station A. Note vertical scale is twice that of horizontal scale.

a systematic check. The Compton kinematics of SLD and this experiment are similar. All the SLD polarimetry equipment has been saved and could be made operational again at relatively low cost. The details of the device and performance are given in Appendix A.

4.4 Target

We plan to use the high power hydrogen target developed for E158. All the components of this target assembly can be re-used in their present configuration, except for the actual target cell itself. The existing liquid hydrogen target uses a 150 cm long cylinder, designed for electrons scattering at < 8 mr and therefore all exiting the downstream endcap. We will shorten the cell length to 100 cm to reduce the sensitivity to higher order radiative corrections and to provide a better match to the spectrometer acceptance. We will use the thinnest possible wall thickness to minimize radiative corrections for electrons exiting near 12 degrees, and re-arrange the flow diverters used to mix the liquid so that they are out of the path of the scattered electrons of interest. Special care will be taken to provide a clean, well-defined geometry for the interface between the cell wall and downstream endcap, as some electrons will pass through this region. The target chamber will be modified to incorporate connections to the two spectrometer vacuum systems. The combination of a shorter cell and higher beam current result in about the same power deposition as in E158, for which the existing refrigerator is adequate.

The liquid hydrogen will be replaced with $> 99\%$ pure liquid deuterium. A careful analysis of the deuterium will be made to determine the percentage of hydrogen and other

contaminants.

The E158 target assembly provides a platform on which a variety of solid targets can be placed. We will use a pair of aluminum targets to measure the asymmetry and rates from the LH2 endcaps, and a set of eight thin carbon targets spaced at 15 cm intervals to verify the acceptance model of the spectrometer (only one target is in the beam at any given time).

4.5 Spectrometers

We propose to build two identical spectrometers to detect electrons scattered near 12 degrees with momenta between 9 and 18 GeV/c. The design is based on the criteria that: a) the detectors be well around a corner from the target; b) the largest possible solid angle be realized; c) only existing magnets be used; d) the acceptance should be optimized for a 100 cm long target; e) that the electron scattering angle be correlated with horizontal position in the detector; f) that there be a vertical momentum focus at the low end of the momentum range (9 GeV), to allow electron identification through E/P_{min} , where P_{min} increases monotonically with vertical detector position.

A design that meets these criteria is shown in Fig. 7. Each spectrometer consists of a vertically focusing quadrupole (Q82-type) followed by a vertically bending dipole magnet (B81 or B82), followed by a second vertically focusing quadrupole (Q82-type). The two dipoles and four quadrupole magnets were originally built for the 8 GeV and 20 GeV spectrometers, and presently are being used in E158 (where they are labeled D2, D3, and Q1-Q4). These magnets were conservatively designed with lots of iron, and have excellent field and gradient uniformity. The design is similar to the 10.5 degree spectrometer built for E155/E155x, except that the present design uses twice the dipole bending power to reduce detector backgrounds. By having the dipole bend downwards, the detectors are close to the End Station floor, thus reducing the cost of building and earthquake-proofing the detector hut. Note that the side plates of the front quadrupoles will be replaced with thinner ones to allow these quadrupoles to be close to the beam pipe. This is a straightforward modification since the side pieces are held in with bolts and are designed to be easily removed. We will avoid large gradient distortions by running these front quads at a pole-tip field of 9 kG, rather than the maximum field of 12.5 kG. The modified quadrupoles will be carefully field mapped, as has recently been done for the un-modified quads for E158. The back quadrupoles will run at a pole tip field of 11 kG, for which the gradient uniformity has been measured to be better than 0.1% over the full radius of 19.3 cm. The dipoles will be run at 90% of their maximum rated field strength to provide good field uniformity (we will use 72 kG-m). These dipole magnets have been extensively studied with Hall probe and long coil field mapping, as well as with a wire float measurement when they were located in the 8 GeV spectrometer.

The power supplies, power cables, and water cooling used for these magnets in E158 will provide the basis for the present proposal. Some power cables will need to be lengthened, and the water plumbing re-arranged. The total power and water consumption will be about 3 MW and 300 Gpm, very similar to the E158 requirements.

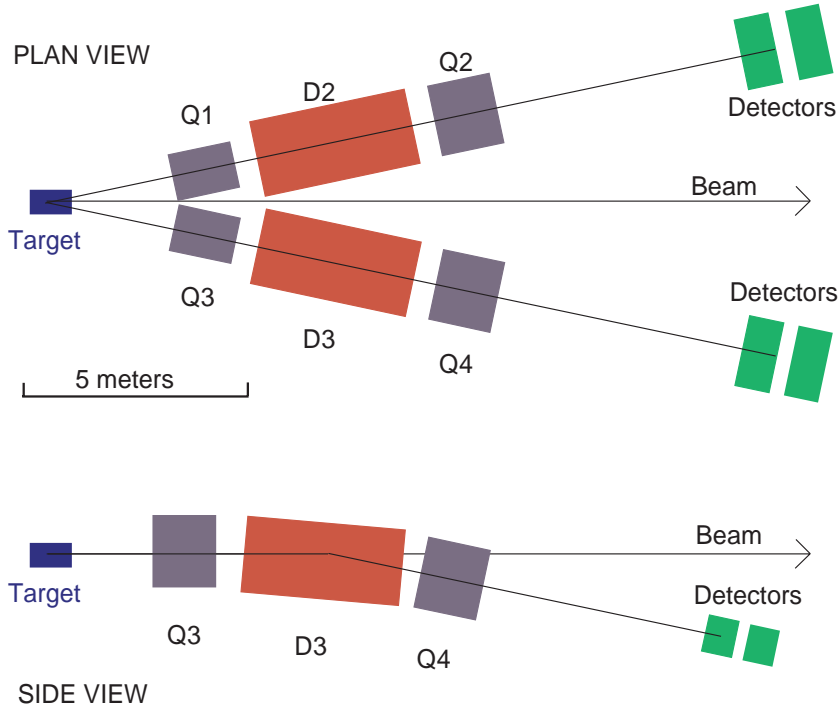


Figure 7: Layout of the two 12 degree spectrometers in End Station A. The target position is near the middle of the hall. The magnet names are the same as in E158.

The spectrometer optics are illustrated in Fig. 8. In the horizontal plane, electrons are defocused, more so at low momentum than high momentum. The acceptance in horizontal scattering angle ranges from ± 8 mr at 9 GeV to ± 12 mr at 20 GeV. The acceptance is relatively insensitive to the scattering location in the projected target length (± 10 cm), although the central scattering angle is correlated with target position, ranging from 11.7 degrees (up-beam end) to 12.3 degree (down-beam end). The horizontal acceptance is cleanly defined by a collimator in front of the detector and another collimator placed between the front quadrupole and the dipole. This minimizes the effects of electrons that scatter on magnet pole faces.

The optics in the vertical plane focuses 9 GeV particles onto the bottom of the detector, as shown in Fig. 9a. Lower momentum particles will not be detected. At higher momenta, the focus moves beyond the detector, resulting in a wider range of momenta at increasing detector vertical position y . However, for each vertical detector layer, there is a minimum momentum P_{min} that increases monotonically with y (i.e. the bottom of the momentum range shown for each row in Fig. 9a). As discussed below, this feature is essential in discriminating pions from electrons. The momentum range is narrowest in the bottom rows, where the pion rates are the largest (as shown in Fig. 9b).

A useful feature of this optical design is that the electron rates are relatively uniformly spread out over the detector in the vertical direction (see Fig. 9b). There will be a small rate variation of about $\pm 15\%$ in the horizontal plane due to the θ^{-4} variation of the cross section. The relatively uniform rates minimize the chance of two electron clusters overlapping in

both space and time and occasionally being counted as a single electron. The probability of two pions overlapping and being counted as an electron will be luminosity dependent, and will be measured using a luminosity scan.

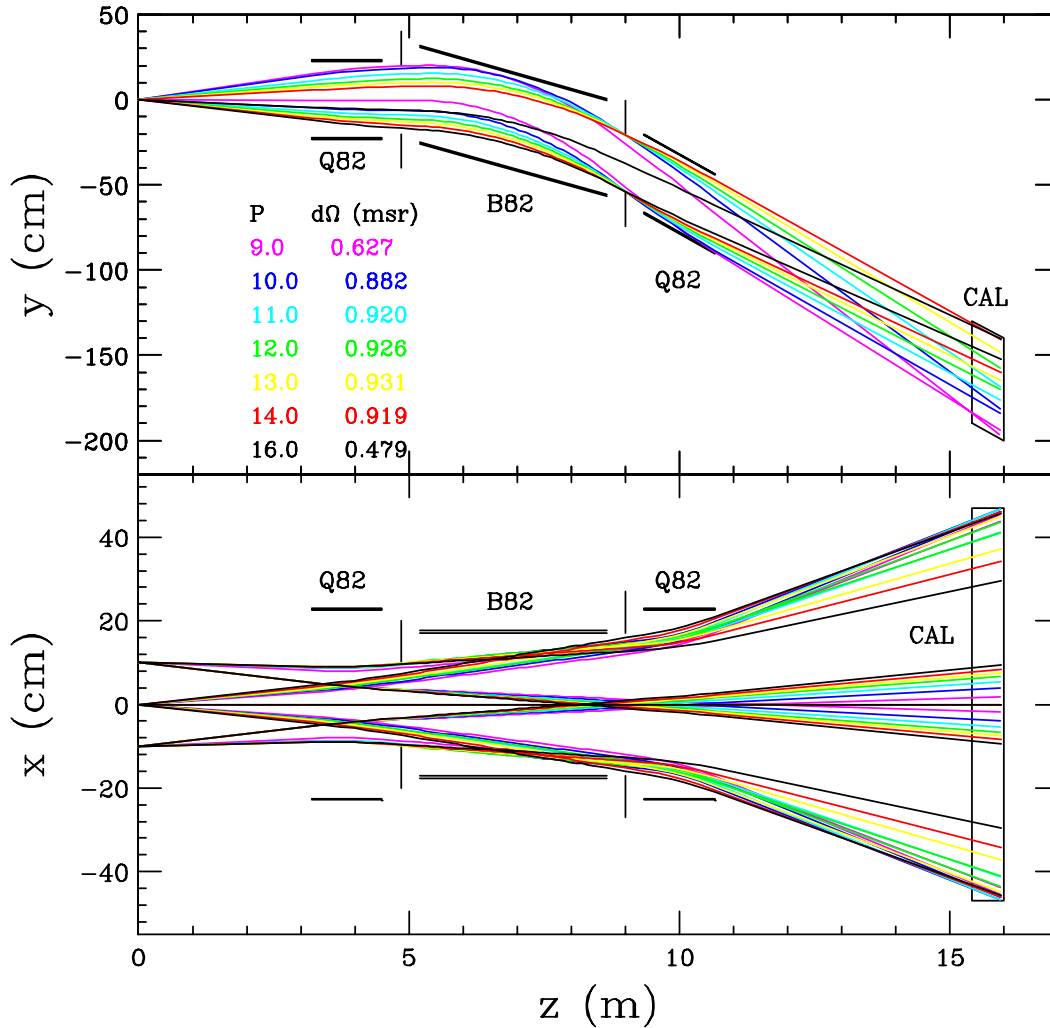


Figure 8: Spectrometer optical properties in the horizontal and vertical planes, for rays with momenta P from 9 to 18 GeV/c, as indicated by the color code in the table listing the solid angle as a function of P in the upper panel. The magnet apertures are indicated, as well as a collimator between the front quadrupole and the dipole. The detector calorimeter is shown where the rays end.

4.6 Detectors

The requirements for the detector system are to cleanly identify and count approximately fifteen electrons per 500 ns beam spill in each spectrometer, and to reject approximately three pions per spill. The detector should be able to measure the electron energy to better

than $\sigma \approx 5\%$, it's position to about 1 cm, and have sufficient granularity that the probability of two electrons overlapping in both space and time is small. A good match to these requirements are the two arrays of 6.3 cm by 6.3 cm by 72 cm lead glass blocks used in a fly's eye configuration in the 2.75 and 5.5 degree spectrometers in the recent E155 experiment. The arrays are 10 blocks high and 20 blocks wide. A fiducial region of 8 by 18 blocks will be defined by a collimator just in front of the detector. Measurements of resolution in a test beam gave $\delta E/E = 0.025 + 0.065/\sqrt{E}$. In actual operation in previous experiments, this detector had an energy resolution of better than 5% for 7 to 40 GeV electrons.

Each horizontal row of blocks detects electrons within a narrow range of momentum due to the focusing properties of the spectrometers. Figure 9a shows this range of momentum. The lower dashed line (E_{min}) is at 85% of the minimum electron energy in that row (more than 3σ below minimum). The energy in each block as a function of time will be recorded by an FADC enabling us to reconstruct clusters of blocks from the electron shower. An electron will deposit, $(94 \pm 3)\%$ of its energy in 4 blocks and almost all of its energy in 9 blocks. The position where the electron hit the detector can be determined to better than 1 cm. Each electron will be cleanly identified by 4 signals from in-time adjacent blocks adding up to greater than $0.94 \cdot E_{min}$ above background. At a rate of approximately 15 electrons/spill (Fig. 9b) there will be one or more overlaps in time (20 ns signal time) and space (> 1 block centroid separation) for 7% of the beam spills. The overlapped clusters can be easily distinguished from single electrons because their total energy will exceed $2E_{min}$, (the upper curve in Figure 9a), which is well above the maximum energy for a single electron in that row. In addition, the time, space, and energy distribution will be different than for a single electron, and the cluster finding routine can be "taught" to distinguish them most of the time. This will reduce the overlap confusion by about a factor of 15 (limited by energy straggling) to 0.5%. The residual overlap dependence can then be measured to 10%. We will use the natural variation of the beam intensity (a few percent) for same helicity pulses to measure the overlap loss (as was done in E158 to measure linearity). This leaves a final dead-time of 0.05%. The variation in the dead-time as a function of rate will then create an uncertainty in A_d of less than 0.1%. This low dead-time counting method largely removes the sensitivity to helicity-dependent detector gain and background levels.

The experimental asymmetry will be determined by counting the number of electron events within the entire detector acceptance for each beam helicity. The average Q^2 needed to compare to the theoretical asymmetry will be determined by convoluting the well-known DIS cross section with the spectrometer acceptance and possible slight variations in counting efficiency. The various empirical fits to the DIS data (including experimental errors) all give the same average spectrometer Q^2 to within 0.05%. The acceptance will be determined by an extensive set of measurements and simulations (see below).

Tests using actual data from E155 have shown that a lead glass calorimeter alone is sufficient to cleanly identify electrons with the proposed optics (similar to the 10.5 degree optics in E155) when the localized π/e ratio is ≤ 1 , as in the present proposal. For additional pion rejection, we will place an array of lead glass blocks behind the electron detector, with two interaction lengths of lead separating the two arrays. The back arrays will consist

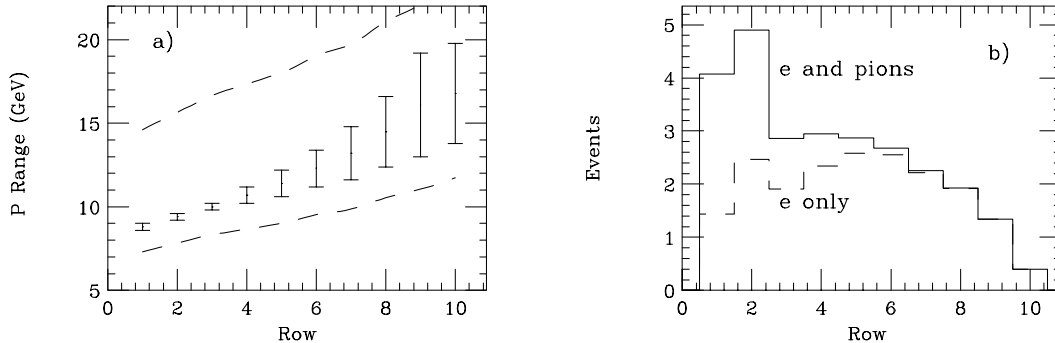


Figure 9: a) Range of electron momenta in the calorimeter detector as a function of row number (1 is the bottom). The lower dashed line (E_{min}) shows $0.85P_{min}$, where P_{min} is the lowest momentum for a given row. Electrons will be identified by a cut $E_{cal} > E_{min}$. Two overlapping electrons will give a signal greater than the upper dashed curve of $2E_{min}$. b) Approximate number of particles per spill as a function of detector row. The dashed line shows electrons only, while the solid line includes pions also. Rows 1 and 10 will be blocked by a collimator.

of 16 blocks (8 blocks wide by 2 blocks tall) each with dimensions 15 cm by 15 cm by 45 cm. These blocks were previously used in E155. The array will be placed to cover the bottom part of the electron detector, where the pion rates are significant. The time coincidence of a small pulse in the front array and a significant signal in the pion array will be used to cleanly identify a large fraction of the pions, and measure the PV asymmetry in their production rate.

4.7 Electronics and Data Acquisition

The signals from the photomultiplier tube mounted on the down-beam end of each block are typically 20 ns long, and will be sent to individual channels of Flash ADC (FADC) with 250 MHz sampling rate. We are currently planning on using FADCs originally developed for the Kamland experiment by Berkeley. They have 128 readouts per channel per trigger and 12-bit resolution per sample. A custom ATWD chip is used with 128 Wilkinson ADCs per chip. Combined with the intrinsic resolution of the lead glass blocks, this will allow energy measurements to better than 5%, and time measurements with 1 ns resolution.

Sufficient high voltage channels and cables are presently available to power the 432 lead glass blocks. Sufficient cables exit to carry the lead glass signals to FADCs. The FADCs themselves will be new items, which will be read out in a VME system. The cost per channel should be reasonable (below \$200/channel), because a large number of similar modules are being built for the Icecube project. After application of the Kamland data compression routine, we expect the raw data count of 100 kB/spill to be reduced to about 30 kB/spill, or 3 MB/sec at 120 Hz. This can readily be accommodated by a modest upgrade to the present E.S.A. data acquisition system. The data rate could be reduced further by not logging FADC channels for which there are no signals above a threshold, set low enough so

Table 2: Kinematics and electron rates as a function of momentum averaged over beam energies of 36 and 39 GeV. The rates are per spectrometer per beam spill. The statistical errors on A_d (relative) and $\sin^2(\theta_W)$ (absolute) are for both spectrometers and beam energies combined.

x	Q^2 GeV ²	Y	E' GeV	W^2 GeV ²	π/e	rate (spill) ⁻¹	dA/A ($\times 100$)	$d\sin^2(\theta_W)$ ($\times 100$)
0.31	15.8	0.89	9.8	36.1	0.86	4.4	1.39	0.14
0.36	17.5	0.86	10.8	32.4	0.23	3.6	1.41	0.15
0.41	19.3	0.83	11.9	28.7	0.06	2.9	1.47	0.16
0.47	21.0	0.79	13.0	25.0	0.02	2.2	1.58	0.17
0.53	22.7	0.76	14.0	21.3	0.00	1.5	1.76	0.20
0.59	24.4	0.72	15.1	17.6	0.00	1.0	2.06	0.24
0.67	26.1	0.69	16.2	13.9	0.00	0.5	2.60	0.30
0.75	27.8	0.65	17.2	10.2	0.00	0.2	3.68	0.44

that there is no loss of true electron or pion data.

4.8 Rates and Statistical Errors

The number of electrons per beam spill per spectrometer is shown in Table 2 for momentum bins that span the spectrometer acceptance. The rates assume a beam current of 9×10^{11} electrons per spill and a target length of 100 cm. Also shown are the kinematic variables x , Q^2 , Y , E' , W^2 , and the expected π/e ratio. All quantities are averaged over equal running times at 36 and 39 GeV. The total rate will be about 15 particles per spill per spectrometer. This is low enough that each electron can be individually counted in the typical spill length of 500 ns. Also listed is the relative statistical error on $A(Q^2)$ and absolute error on $\sin^2(\theta_W)$ assuming a beam polarization of 0.85, 4×10^8 spills of data on tape, a 90% beam quality efficiency, and adding both spectrometers together. Combining the bins together results in a relative error of 0.6% on $A(Q^2)$ and ± 0.0006 on the extracted value of $\sin^2(\theta_W)$.

4.9 Optimal Repetition Rate

The accelerator systems can be set to provide beams at 30, 60, or 120 Hz. The incremental power needed depends on whether the experiment is run stand-alone or simultaneously with PEP-II. We assume an effective beam delivery efficiency of 75% for stand-alone running, and 50%, 62%, and 68% for running with PEP-II at 30, 60, or 120 Hz, based on experience during recent E158 running. We assume an additional inefficiency of 15% due to experimental down time. The A-line will use 1.1 MW for the average of 36 and 39 GeV running, the Compton polarimeter will use about 0.9 MW, and the two spectrometers (combined) will use about 3 MW. The linac power needed is $0.1ER/30$ for stand-alone running, where E is the beam energy in GeV and R is the repetition rate in Hz. This corresponds to 3.8, 7.6, and 15.4

Table 3: Total number of hours and GW-hr needed to obtain 5×10^8 pulses at an average beam energy of 37 GeV for the repetition rate and running mode indicated.

	with PEP-II		stand-alone	
R	Hours	Energy	Hours	Energy
30 Hz	9258	46.3 GW-hr	6172	48.1 GW-hr
60 Hz	3703	32.5 GW-hr	3086	35.8 GW-hr
120 Hz	1683	28.0 GW-hr	1543	30.0 GW-hr

Table 4: Estimated experimental systematic errors on dA_d/A_d and $\sin^2(\theta_W)$.

source	dA_d/A_d	$d\sin^2(\theta_W)$
Beam Polarization	0.003	0.0003
Kinematic determination of Q^2	0.003	0.0003
Electromagnetic radiative corrections	0.003	0.0003
False asymmetries	0.001	0.0001
Pion contamination	0.001	0.0001
Pair symmetric background	0.001	0.0001
Target purity, density fluctuations	0.001	0.0001
Electronics dead time and pile up effects	0.001	0.0001
total	0.006	0.0006

MW at 30, 60, and 120 Hz. The linac power for concurrent running with PEP-II is reduced by 2.8 MW, corresponding to 1.0, 4.8, and 12.6 MW at 30, 60, and 120 Hz. The incremental electrical power and calendar hours needed to obtain 5×10^8 pulses are given in Table 3 for different repetition rates and running modes. The most efficient mode will depend on the cost structure for electricity at the time of running.

5 Experimental Systematic Errors

Experimental systematics affect both the relative error on the measured values of dA_d/A_d and the values of $\sin^2(\theta_W)$ extracted from A_d . A summary is given in Table 4, and detailed discussions of each source of uncertainty are given in the following sub-sections.

5.1 Beam Polarization

As discussed below, we plan to measure the beam polarization continuously in End Station A using the SLD [22] Compton polarimeter. This device operated with an overall uncertainty of 0.5% at SLD. The shorter laser transport line and anticipated lower and

more stable backgrounds in ESA lead us to expect that we should also be able to achieve a smaller uncertainty of 0.3%. The additional of a recoil photon detector will provide a valuable systematic check. The beam polarization enters as a straight multiplicative factor into A_d , leading to a 0.3% uncertainty in dA/A , corresponding to an uncertainty of 0.0003 in $\sin^2(\theta_W)$.

5.2 Kinematic Determination of Q^2

Since the measured asymmetries are directly proportional to Q^2 , we need to know the effective average $Q^2 = 4EE' \sin^2(\theta/2)$ with an accuracy of better than 0.3% in order not to dominate over the statistical errors. This will require accurate knowledge of the beam energy E , and the correlated average scattered electron energy E' and angle θ , since $Q^2 = 4EE' \sin^2(\theta/2)$.

5.2.1 Beam Energy

The incident beam energy E in E.S.A. is known to better than 0.1% from careful calibration of the A-line magnets. It will be checked, as has been done in the past, by measuring the longitudinal beam polarization as a function of energy in small steps between 36 and 39 GeV. The zero crossing point accurately defines a beam energy of 37.22 GeV (11.5 $\pi/2$ precessions in a bend angle of 24.5 degrees). The effects of synchrotron radiation in the A-line will be accounted for in the standard way. Thus beam energy will contribute an uncertainty in Q^2 of less than 0.1%.

5.2.2 Scattered Angle and Momentum

The other uncertainty arises from measuring the average $E' \sin^2(\theta/2)$ in the spectrometer. This is determined by the apertures that define the acceptance as well as by the spectrometer optics. Careful alignment will allow the central angle θ to be defined to 0.2 mr, corresponding to an uncertainty in Q^2 of 0.2%. The tests outlined below will allow a determination of E' to 0.2%, corresponding to a 0.2% uncertainty in Q^2 . The total error in average Q^2 is then 0.3%.

We propose to make a wire-float measurement of the acceptance and optical properties of each spectrometer. The technique uses a light, current-carrying wire to simulate the trajectories of particles. A wire float measurement of the 8 GeV spectrometer (composed of a superset of the magnets for the present proposal) was performed in the 1980's [23] as part of Experiment E140. In general it showed excellent agreement with the design optics model, but did reveal some subtle differences. The central angle of that spectrometer was determined to ± 0.05 mr and the central momentum to $\pm 0.04\%$. In addition, the magnet control system was measured to be stable to $\pm 0.03\%$. The optics coefficients were determined to an accuracy which enabled us to determine the acceptance to $\pm 1\%$. The optical model built on the wire float measurements was able to predict the position of the elastic peak in $e + p \rightarrow e + p$ to within 0.13% in momentum (well within our tolerance of $\pm 0.2\%$). A wire float measurement of the present spectrometers will be easier because they

are shorter (one dipole instead of two, and two quads instead of three), bend towards the floor rather than the ceiling, and are fixed in position rather than movable on a carriage.

As a cross check we will make detailed field maps of the magnets and compare the predicted trajectories with the the wire float measurements.

We will create a detailed spectrometer model based on the measured field maps of the magnets, wire float, and surveyed position of all components. This will be checked against several types of calibration runs:

- A set of thin carbon foils at various positions along the beam axis will be used to verify the target-position dependence of the acceptance.
- The relative counting rate as a function of vertical and horizontal position at the detector will be compared to the predictions from the global fits to the structure functions F_2 and R . This will give a detailed picture of the effects of optics as well as the way various collimators effect the acceptance. These global fits, weighted by acceptance, can be used to determine the average Q^2 of the spectrometers. The cross sections in our kinematic region have been measured by SLAC, NMC and BCDMS and are well known. Differences between nine different global fits, (including upper and lower experimental limits on some fits) give $\delta Q^2/Q^2 \leq 0.05\%$.
- Tests using an aperture-defining mask in front of the first quadrupole will define an otherwise aperture-free set of rays using a point target.
- Cross sections will be measured with the quadrupoles both turned on and off to set limits on the effects of quadrupole mis-alignment and gradient non-linearity.
- A series of measurements will be made with beam energies from 12 to 25 GeV in 1 GeV steps. This essentially sweeps the largest kinematically allowed E' values across the spectrometer acceptance. Since the shape near the endpoint is well known, this provides a very powerful set of constraints on the optics model.

We have begun a program of simulations of the above tests and varying parameters such as magnetic field parameterizations, target, collimator, and magnet position alignments, amount of scattering from apertures, the amount of low energy background, and other effects. Note that A_d has very little sensitivity to detector position because the number of events is determined by collimators in front of the detector. There is also little sensitivity to the detector energy calibration, other than the slight variation in inefficiency from electron shower tails that fall below the E_{min} cut for a given row in the counter. Preliminary indications are that the kinematic determination of Q^2 to 0.3% will be achievable. Additional optics and background checks are being considered.

5.3 Electromagnetic Radiative Corrections

Electromagnetic radiative corrections arise from the emission of photons by either the incident or scattered electron, either in the field of the nucleus (internal corrections), or in

the field of another nucleus (external corrections). The ratio R_U of radiated to un-radiated spin-averaged cross sections is shown in Fig. 10a as a function of x for a beam energy $E = 39$ GeV and electron scattering angle $\theta = 12$ degrees. At low x , the radiated cross section is larger than the Born cross section, while the reverse is true at high x . In the kinematics of this proposal, contributions from quasi-elastic and elastic scattering in the deuteron are negligible ($< 0.2\%$ in the lowest x bin), so that R_U is essentially determined by the (x, Q^2) dependence of the spin-averaged structure function F_2 . Of particular relevance is the ratio R_P of radiated to un-radiated ed parity-violating asymmetry shown in Fig. 10b. This ratio is close to unity at high x , and decreases slowly at low x , due to the decrease in average Q^2 at the scattering vertex. The shape and magnitude of R_P is primarily determined by the probability for an electron to radiate a hard photon in deuterium, and to a lesser extent by the (x, Q^2) dependence of F_2 and A_d . Fig. 10c shows the fractional errors on A_d due to uncertainties in the radiative corrections. These systematic errors are less than 0.4% for $x > 0.3$, with weighted average of about 0.3% . They are primarily due to uncertainties in the structure function F_2 as represented in various fits to world data. Uncertainties in the target dimensions and various windows which act as radiators have much smaller effects. These calculations were performed in the peaking approximation of Mo and Tsai [24]. Calculations with the more exact formulas of Ref. [25] are underway.

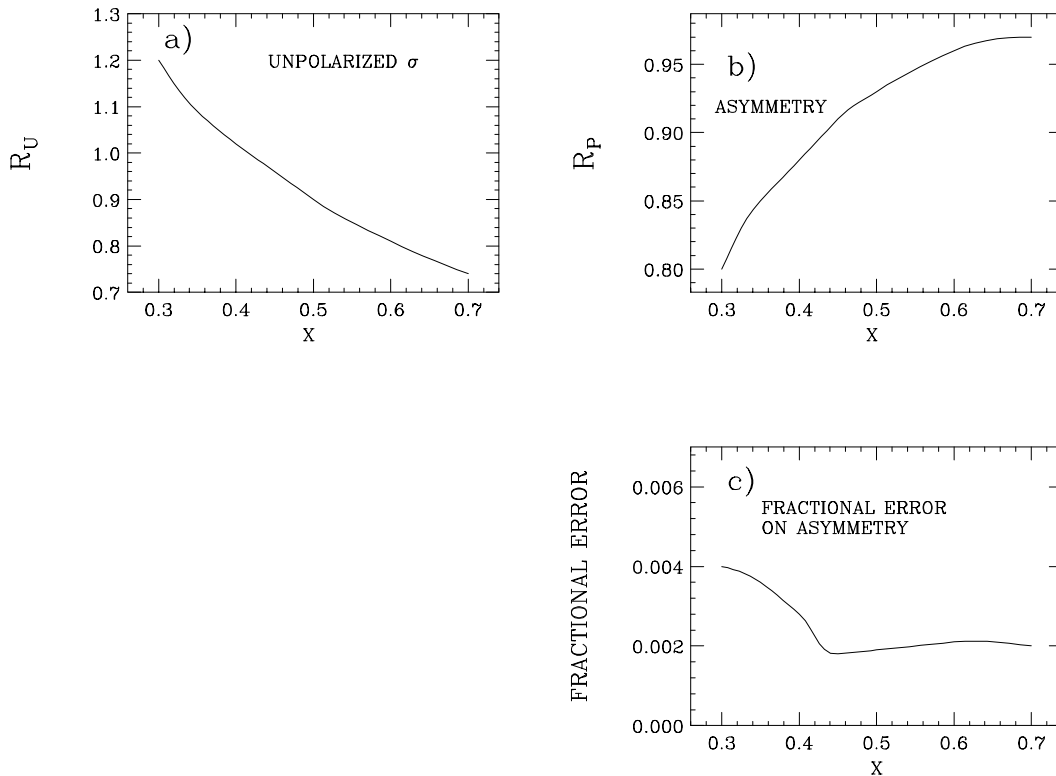


Figure 10: Radiative correction as a function of x . a) The ratio of measured to Born cross sections (R_U); b) The ratio of measured to Born asymmetries (R_P); c) The fractional error on the Born asymmetry.

5.4 False Asymmetries

Asymmetries in beam parameters will lead to changes in the measured physics asymmetries for which corrections must be made. Fortunately, the E158 collaboration has introduced many improvements to beam diagnostics and feedback systems which have led to very small and well-measured beam asymmetries. With active feedback, the charge asymmetry can be kept below 1 ppm (parts per million), and measured to better than 10 ppb (parts per billion), averaged over 10^8 beam spills. Since the physics asymmetry will be of order 2000 ppm, the error from beam charge asymmetry is negligible. The average energy asymmetry in Run I of E158 was 2.0 ± 1.4 KeV [26], which leads to a physics asymmetry correction of only 40 ppb due to the difference in average Q^2 for the two helicity states. The average helicity-correlated x and y position differences at the target were found to be of order 10 ± 5 nm in E158, corresponding to helicity-correlated differences in Q^2 of less than 10 ppb for the present experiment. The average angle differences in E158 were found to be of order 0.5 ± 0.2 nrad, leading to a Q^2 differences of less than 5 ppb. Thus both the size and errors on the position and angle corrections are negligible for A_d . In this regard, the present experiment benefits from a much larger scattering angle than E158 (12 degrees compared to 0.3 degrees). In addition, the left-right symmetry of the two spectrometers will to first order cancel the x angle and position beam asymmetries. In summary, beam-related false asymmetries will contribute less than 0.1% to the relative uncertainty on A_d .

5.5 Pion Contamination

The predicted π/e ratios shown in Table 2 are based on a fit to pion photoproduction data [27], which has proven to be accurate to 20% or better in past experiments. The π/e ratio is strongly x -dependent, approaching 1 in the lowest x bin. Averaged over the spectrometer acceptance, the ratio is predicted to be about 0.1. We will measure the π/e with an accuracy of better than 10%. Using only the front electromagnetic calorimeter, we expect to reject 95% of the pions, based on experience in E142-E155. About two thirds of the remainder will be rejected by a time-coincident signal in the pion detector, resulting in less than 2% of pions being mis-identified as electrons. Scaling this by the π/e ratio of 0.1, this will leave a pion contamination of about 0.2% to the electron signal. Assuming the pion asymmetry is small compared to the electron asymmetry, this leads to a 0.2% dilution to A_d , with a relative systematic uncertainty of less than 0.1%. The pion asymmetry will be verified to be small, as already seen in the original SLAC experiment [2], because most pions will be cleanly identified from a front/back detector coincidence. While we don't know of any calculations of the pion photoproduction asymmetry at our kinematics, the predicted asymmetry is of order 10^{-7} at energies below 0.55 GeV [28], and 1.3×10^{-6} for excitation of the $\Delta(1232)$ resonance [29]. These are both negligible compared to our expected electron asymmetry of about 2×10^{-3} .

5.6 Pair Symmetric Background

In addition to the DIS events of interest, electrons can originate from decays of vector and pseudo-scalar mesons, and wide angle pair production. To a very good approximation, these processes are pair-symmetric, and can be measured with better than 3% accuracy by reversing the polarity of the spectrometers. Based on simulations with PYTHIA [30], we expect the largest source of pair-symmetric events to be from decays of photoproduced J/ψ and π^0 mesons. The simulation is in reasonable agreement with data taken in E155 at 10.5 degrees with a beam energy of 48.3 GeV (close to the kinematics of the present proposal). The predicted e^+/e^- ratio for this proposal varies from 3% at $x = 0.3$ to $< 0.01\%$ for $x > 0.5$, with an average ratio of 1%. The asymmetry is expected to be very small, and this will be verified by taking data for approximately 3×10^7 beam pulses with reversed spectrometer polarity. The net relative uncertainty on A_d will be $< 0.1\%$.

5.7 Target Purity and Density Fluctuations

Based on previous experience, the largest contamination of the liquid deuterium target is from hydrogen, with a typical value of $1 \pm 0.3\%$. In the proposed kinematics, the asymmetry from hydrogen is about 25% smaller than for deuterium, on average, leading to a systematic uncertainty of $< 0.1\%$ on dA_d/A_d . Since the asymmetry from other possible contaminants (such as nitrogen and oxygen) is essentially the same as for deuterium, their net effect is negligible. The asymmetry for the aluminum target windows is predicted to be slightly larger (by about 2%) than for deuterium, which results in a negligible asymmetry error as the window thickness will be known to better than 0.01 gm/cm^2 (to be compared to the 16 gm/cm^2 in the liquid deuterium target).

Studies performed in E158 [31] have shown that the effective target density as a function of beam current is well understood, and helicity-correlated effects arising from beam spot-size, energy, and intensity fluctuations are at the level of 20 to 70 ppm per pulse pair, and less than 10 ppb averaged over 10^8 pulses. The corresponding effect on A_d is 0.01% (relative error), which is essentially negligible. The introduction of a skew quad into the A-line optics for E158 [32] was crucial to reduce the vertical spot-size jitter to the presently observed level. The spot-size jitter will be somewhat larger in the present proposal than for E158 due to the higher proposed beam current, but this will mostly be compensated for by using a larger beam spot size than was possible in E158 (2 mm radius compared to 1 mm).

5.8 Electronics Dead Time and Pile Up Effects

By using Flash ADCs to read out all of the detectors, the effects of dead time and overlapping signals (pile up) are greatly reduced compared to our previous reliance on TDC's. We anticipate that about 0.5% of the electron showers of interest will overlap in both space and time with another shower from a pion or electron, causing confusion in the electron counting. The effects will be studied by varying the beam current, and modeled with Monte Carlo simulations. Preliminary studies indicate that corrections can be made with an accuracy of 0.1% on A_d .

Table 5: Estimated absolute theoretical systematic errors on extracted values of $\sin^2(\theta_W)$.

source	$d\sin^2(\theta_W)$
Dynamic higher twist	0.0001
Electroweak radiative corrections	0.0002
Uncertainty in quark distributions	0.0002
Charge symmetry violation	0.0002
Uncertainty in R	0.0001
total	0.0004

6 Theoretical Systematic Errors

Theoretical systematic errors affect the value of $\sin^2(\theta_W)$ extracted from the measured value of A_d/Q^2 . These uncertainty are difficult to estimate and also time-dependent, in the sense that they can be reduced as further information from other experiments becomes available (for example, better measurements of the sea quark distributions or higher twist effects). Our best estimate of the principal theoretical errors is summarized in Table 5 and detailed in the following sub-sections.

6.1 QCD and Higher-Twist Corrections

Dynamic higher twist diagrams can make significant contributions to lepton scattering amplitudes at low Q^2 . They arise from correlations among the quarks and gluons. The order of twist n is characterized by a $1/Q^{n-2}$ falloff (at fixed x or W) relative to the leading twist-2 amplitude considered in Eq. 7 for A_d . We would therefore expect twist-four contributions to dominate at high Q^2 , compared to twist-six or higher. An explicit calculation of twist-four effects on A_d was made in 1985 by Castorina and Mulders [33]. Using MIT bag-model parameters, they found the maximum effect on the extracted value of $\sin^2(\theta_W)$ is less than 0.001 at $Q^2 = 2 \text{ GeV}^2$, and less than 0.0001 at $Q^2 = 20 \text{ GeV}^2$. Assuming a 100% uncertainty in their calculation gives a systematic error of 0.0001 to the higher twist correction.

Another way to obtain an upper bound is to look at higher twist effects on the spin-averaged cross section, since we can reasonably expect the effects to mostly cancel in the asymmetry ratio. A recent phenomenological study [34] examined the effects of higher twist on the moments $M_n(Q^2)$ of the unpolarized structure function F_2 , where $M_n(Q^2) \approx \int_0^1 x^{n-1} F_2(x) dx$ at large Q^2 . The study showed that the sum of twist-4, twist-6, and higher twist effects contributes less than 1% to the M_2 , M_4 , and M_6 moments at $Q^2 = 20 \text{ GeV}^2$.

6.2 Electroweak Radiative Corrections

The electroweak radiative corrections are very well determined in the Standard Model. They are similar to the corrections for atomic parity violation determined by Marciano and Sirlin [35], except at higher Q^2 . The overall correction to our measured asymmetry A_d is less than 1%.

The corrections modify the ρ , κ , and λ parameters in Eq. 5 from their tree level values. A recent evaluation [15] at very low Q^2 of the corrections gives $\rho' = 0.9878$, $\rho = 1.0007$, $\kappa' = 1.0027$, $\kappa = 1.0300$, $\lambda_{1d} = -2\lambda_{1u} = 3.7 \times 10^{-5}$, $\lambda_{2u} = -0.0121$ and $\lambda_{2d} = 0.0026$. At our kinematics, the values are slightly different due to the Q^2 dependence

The calculations depend on well-known Standard Model parameters such as α , M_Z and M_W , on the Higgs scale (very weakly), on the momentum transfer, and on $\sin^2(\theta_W)$ itself. All terms are of order $\alpha/(2\pi)$ and thus small.

The corrections come from several different types of diagrams.

- Running of $\sin^2(\theta_W)$ due to γ -Z mixing giving a well-understood correction at $Q^2 = 20 \text{ GeV}^2$ [36].
- Axial-vector renormalization, which is small and well-understood compared to the Q^2 of APV [37].
- Anapole moment contribution, which is negligible for DIS at $Q^2 = 20 \text{ GeV}^2$ since the scattering is from individual quarks [38].
- Charge-radii where the photon couples to intermediate photons, which has an approximately 0.1% effect on A_d [36].
- WW and ZZ box diagrams, whose contribution has an uncertainty of at most a 0.1% on A_d [36].
- γZ box diagram, which has an uncertainty of less than 0.1% on A_d [36].

The calculation is easier at our Q^2 than at the scale of the APV experiments [37]. For DIS, Q^2 determines the size of propagators for the light quarks rather than estimates of their effective masses [36, 37]. The same holds for the onset of the γZ box diagram. In addition, since in DIS the scattering is off individual quarks, the axial-vector current contributions to the nucleons are irrelevant.

In summary the electroweak radiative corrections are small and can be calculated with confidence to an accuracy which effects A_d by less than about 0.2%.

6.3 Uncertainty in Quark Distributions

The quark distributions enter the calculation of A_d (Eq. 7) through R_c , R_s , and R_v defined in Eq. 8. In the region where the sea quarks are negligible, $R_c = R_s = 0$ and $R_v = 1$. The quark distributions in nucleons have been parameterized by many groups (MRS, GRV, CTEQ) using the pQCD evolution equations. Fits done up to the year 2000 are summarized

in the CERN library [39]. More recent results from MRST [40] and CTEQ [41] have also been used. The later also include estimates of the errors. We have estimated the errors on A_d from the uncertainty in the quark distribution in four ways. a) the error from the MRST parameterization; b) the error from the CTEQ parameterization; c) the root mean square of the distribution of over twenty different parameterizations; and d) the maximum deviation of any of the models from the mean of all the models. In each case, we included the two alternatives of full charm quark suppression or no suppression. The relative uncertainty on $\sin^2(\theta_W)$ from all four methods are shown in Fig. 11. The largest of these uncertainties at each value of x is usually the CTEQ error estimate. The maximum deviation method error at low x is due to the CTEQ5M (no c quark) being most different. The average largest uncertainty on $\sin^2(\theta_W)$ (weighted by the statistical error as a function of x) is about 0.0002, which is dominated by uncertainty in the charm sea distribution, especially at higher x .

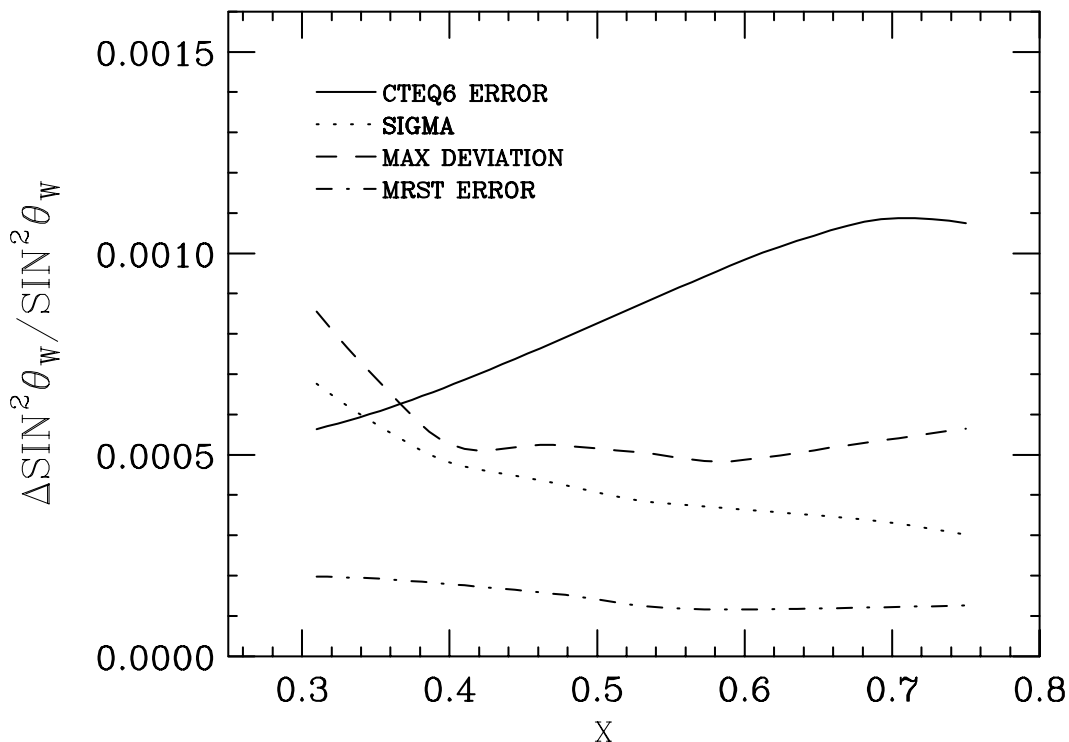


Figure 11: Relative systematic error on $\sin^2(\theta_W)$ due to uncertainty in the quark distributions as a function of x . Four different methods described in the text were used to calculate the uncertainty.

We did not include in our systematic study the parton distributions of Alekhin [42] because they only fit DIS data, and their sea quark distributions conflict with Drell-Yan data. We did not include the PDFs from [43] because they only fit a subset of the data usually used in global PDF analyses, providing less constraints on R_s , R_v , and R_c .

Additional corrections at high x can arise from nuclear modifications [44] to the PDFs in a deuteron compared to the average of a free proton and neutron. In leading twist, only the ratios R_s , R_c , and R_v are affected. Since R_s , R_c and $1 - R_v$ are close to zero, and nuclear

corrections to these quantities are expected to be smaller than the present uncertainties in the ratios, the net effect on $\sin^2(\theta_W)$ is probably below 0.0001.

6.4 Charge Symmetry Violation

Equation 7 assumes that the proton and neutron are charge symmetric, i.e. that the quark distributions $\delta u \equiv u^p - d^n = 0$, $\delta d \equiv d^p - u^n = 0$, $\delta s \equiv s^p - s^n = 0$ and similarly for anti-quarks. Charge symmetry is not strictly true [45], since the mass of the down quark is greater than the mass of the up quark ($m_d/m_u \approx 1.8$, $m_d - m_u \approx 3$ MeV). However, this difference is only 1% of the relevant strong Hamiltonian energy of about $m_\rho/2$. Thus naively we expect that the $\delta q/q$ to be less than 1%. This is not borne out at high x in some models.

If there is a charge symmetry violation (CSV) for the u , d and s quarks, then Eq. 7 would be replaced by:

$$A_d \propto \frac{2C_{1u}[1 + R_c - R_{\delta d}] - C_{1d}[1 + R_s - R_{\delta u} - R_{\delta s}] + Y(2C_{2u} - C_{2d})(R_v - \frac{R_{v\delta u}}{3} - \frac{2R_{v\delta d}}{3})}{[5 + R_s + 4R_c - R_{\delta u} - 4R_{\delta d} - R_{\delta s}]} \quad (17)$$

where

$$\begin{aligned} R_{\delta d} &= \frac{\delta d(x)}{u(x) + d(x)} \\ R_{\delta u} &= \frac{\delta u(x)}{u(x) + d(x)} \\ R_{\delta s} &= \frac{\delta s(x)}{u(x) + d(x)} \\ R_{v\delta u} &= \frac{\delta u_v(x)}{u(x) + d(x)} \\ R_{v\delta d} &= \frac{\delta d_v(x)}{u(x) + d(x)}. \end{aligned} \quad (18)$$

Equation 17 reduces to Eq. 7 when all terms defined in Eq. 18 are zero.

Both the MIT bag model [45, 46, 47] and the Meson Cloud model [48] have been used to calculate CSV. Within the bag model several effects could contribute to a CSV [45] including the proton neutron mass difference of 1.3 MeV (small), the difference of masses of the intermediate states (large), and various changes in bag parameters (small). The biggest effect is due to the difference in the mass and charge of the 2-quark intermediate state which for u^n is two down quarks while for d^p is two up quarks. This leads to effects of up to 7% at $x=0.7$, which fortunately are partly cancelled by some of the other effects.

We have used four different calculations of CSV for the valence quarks [45, 46, 48, 47], and two different calculations for the sea quarks [48] to see if CSV affects the interpretation of our results. These same models were used by the NuTeV experiment [6] to evaluate corrections to their measurement of $\sin^2(\theta_W)$. The most extreme of these models [45] at high x has a $\delta d_v^p \sim 5\%$ of the average valence quark and would change the average extracted

value of $\sin^2(\theta_W)$ by 0.0005. Averaging over the models and x gives a relative correction of $0.1\% \pm 0.1\%$ (or 0.0002 ± 0.0002 absolute).

6.5 Uncertainty in $R = \sigma_L/\sigma_T$

The structure function R enters into the asymmetry calculation through the quantity Y (Eq. 2). The R1998 fit [49] yields values of R ranging from 0.03 to 0.06 over the kinematics of this proposal, with an error estimate of 0.023 to 0.025. Since the coefficient in front of Y in Eq. 10 is small, this corresponds to a systematic error on $\sin^2(\theta_W)$ of 0.00015 at low x , decreasing to 0.00004 at high x , with an average weighted value of 0.0001.

7 Manpower, Schedule, and Summary

Most of the members of this collaboration have had extensive experience in setting up custom spectrometers in End Station A. In particular, we have a lot of experience using the proposed Q82-type quadrupoles and B81-type dipoles. We have extensive experience with the specific lead glass detectors we propose to use, as well as experience in data analysis using FADC readouts. Members of the collaboration have been heavily involved in the ongoing E158 experiment, which has achieved beam parameters that match or exceed the requirements of the present proposal. Collaboration members have also been involved in the design and operation of the SLD Compton polarimeter.

We believe that the polarimeter, target, spectrometers and detectors could be set up in E.S.A. within 18 months of approval, because essentially all the major components of these systems are existing devices. The fabrication, and testing of the FADCs should also be finished within 18 months. We would expect to be ready for a commissioning run by the end of 2005, and production running some months later (depending on what problems are uncovered).

In summary, we propose a precision measurement A_d using deep-inelastic parity violating electron scattering from deuterium. We expect to extract $\sin^2(\theta_W)$ with a statistical error of 0.0006, an experimental systematic error of 0.0006, and a theoretical systematic error of 0.0004, for a total error of 0.0009. This will be a very competitive determination of $\sin^2(\theta_W)$ away from the Z -pole, and provide significant constraints of the existence and characteristics of physics beyond the Standard Model. We request resources to assemble the polarimeter, target, spectrometer, detector, and electronics. Our beam time request is summarized in Table 6.

Table 6: Summary of beam request

Energy (GeV)	Purpose	Beam Spills
35.6	Production	2×10^8
38.8	Production	2×10^8
35.6	e^+ Background	3×10^7
12 to 38	Energy Scan	3×10^7
35.6	Checkout	4×10^7
total		5×10^8

8 Appendix A. Compton Polarimeter

In spin-dependent Compton scattering, circularly polarized laser photons interact with the electron beam so that the photon energy in the electron rest frame is several hundred KeV. The spin dependence of Compton scattering leads to a large difference in scattered electron count rate which is proportional to the electron polarization. Compton polarimetry is the best choice for precision polarimetry for several reasons: i) the physics of the scattering process is well understood QED, with radiative corrections less than 0.1% [50]; ii) detector backgrounds are easy to measure and correct for by using "laser-off" pulses and "electrons-off" pulses; iii) polarimetry data can be taken parasitic to physics data; iv) the Compton scattering rate is high and small statistical errors can be achieved in a short amount of time (sub-1% precision in a few minutes is feasible); v) the laser helicity can be selected on a pulse-by-pulse basis; and vi) the laser polarization can be greater than 99.8% and is readily determined with 0.1% accuracy.

In the electron rest frame the spin-dependent Compton cross section is given by [51]

$$\begin{aligned} \frac{d\sigma}{d\Omega} = & \frac{r_e^2 q^2}{2 q_0^2} \left[(1 + \cos^2 \theta) + \frac{(q_0 - q)}{m} (1 - \cos \theta) \right. \\ & \left. \pm P_e^L P_\gamma (1 - \cos \theta) \frac{(q_0 + q)}{m} \cos \theta \right. \\ & \left. \pm P_e^T P_\gamma \cos \phi (1 - \cos \theta) \frac{q}{m} \sin \theta \right] \end{aligned}$$

where q_0 and q are the incident and scattered photon energies in the electron rest frame ($q_0 = 2E \frac{\lambda_C}{\lambda}$) with $\lambda_C = 2.43 \times 10^{-3}$ nm the electron Compton wavelength, λ the laser wavelength measured in the lab frame, and E the electron beam energy in the lab frame. θ and ϕ are the polar and azimuthal scattering angles of the photon with respect to the incident photon. The + and - refer to electron and photon helicities parallel and anti-parallel. (Both the electron and photon helicities can be changed on a pulse-to-pulse.) The electron polarization components are separated into longitudinal (P_e^L) and transverse (P_e^T) pieces. In the lab frame, the cross section for longitudinal electron polarization can be

written (averaging over azimuthal angles) as

$$\frac{d\sigma}{d\rho} = \frac{d\sigma_0}{d\rho} \pm P_e^L P_\gamma \frac{d\sigma_1}{d\rho}$$

$$\frac{d\sigma_0}{d\rho} = r_e^2 a \left[1 + \frac{\rho^2(1-a)^2}{1-\rho(1-a)} + \left(\frac{1-\rho(1+a)}{1-\rho(1-a)} \right)^2 \right]$$

$$\frac{d\sigma_1}{d\rho} = r_e^2 a \left[(1-\rho(1+a)) \left(1 - \frac{1}{(1-\rho(1-a))^2} \right) \right]$$

where

$$\rho = q/q_{max}$$

and q and q_{max} are the final and maximum final photon energies in the electron rest frame given in terms of the electron energy E (in the lab frame) by

$$q_{max} = E(1-a) \quad \text{and} \quad a = \frac{1}{1+4\gamma\lambda_C/\lambda}.$$

where γ is the boost from lab to electron rest frame.

The primary polarization measurement will come from rate asymmetry measurements of the Compton-scattered electrons. The analyzing power spectrum of Compton-scattered electrons is shown in Fig. 12a, for an electron beam energy of 39 GeV and laser wavelength of 532 nm, as a function of scattered electron energy in the lab E' . As in the SLD Compton polarimeter, we will measure the asymmetry spectrum of Compton-scattered electrons between the Compton edge (at 16 GeV) and the zero-crossing point (at 23 GeV). The counting rate per spill for a beam intensity of 9×10^{11} /spill, a laser power of 0.05 J/spill and a crossing angle of 10 mr is shown in Fig. 12d. The rate is over 20 electrons/GeV/spill, and is a maximum where the analyzing power is greatest.

The electron polarization can be determined from the asymmetry in rates for electron and photon spins parallel ($N_i^{\uparrow\uparrow}$) and anti-parallel ($N_i^{\uparrow\downarrow}$). The measured asymmetry in detector channel i , is given by:

$$A_i^m = \frac{N_i^{\uparrow\uparrow} - N_i^{\uparrow\downarrow}}{N_i^{\uparrow\uparrow} + N_i^{\uparrow\downarrow} - 2N_i^{off}} = a_i P_e P_\gamma,$$

where N_i^{off} is the laser-off background rate. The detector channel's analyzing power, a_i , is determined from the analyzing power spectrum $A(x)$ shown in Fig. 12b and the detector channel's response function, $R_i(x)$,

$$a_i = \frac{\int \frac{d\sigma_0}{dx} A(x) R_i(x) dx}{\int \frac{d\sigma_0}{dx} R_i(x) dx}$$

The scheme for detecting the scattered electrons is shown in Fig. 6. It is very similar to that employed by SLD. The optimum location for the laser has not yet been finalized. The laser beam crosses the incident electron beam at an angle of 10 mr at a point several meters

upstream of a set of chicane magnets. The soft bend and first large chicane magnet are used to momentum-analyze the Compton-scattered electrons. Energy resolution of the scattered electrons is provided by the segmented SLD Čerenkov detector. The major elements of the Compton polarimeter are 1) the laser and optics, 2) the chicane for dispersing the beam and Compton-scattered electrons, and 3) the position-sensitive detector for the Compton-scattered electrons. Each of these is discussed in more detail in the next sections.

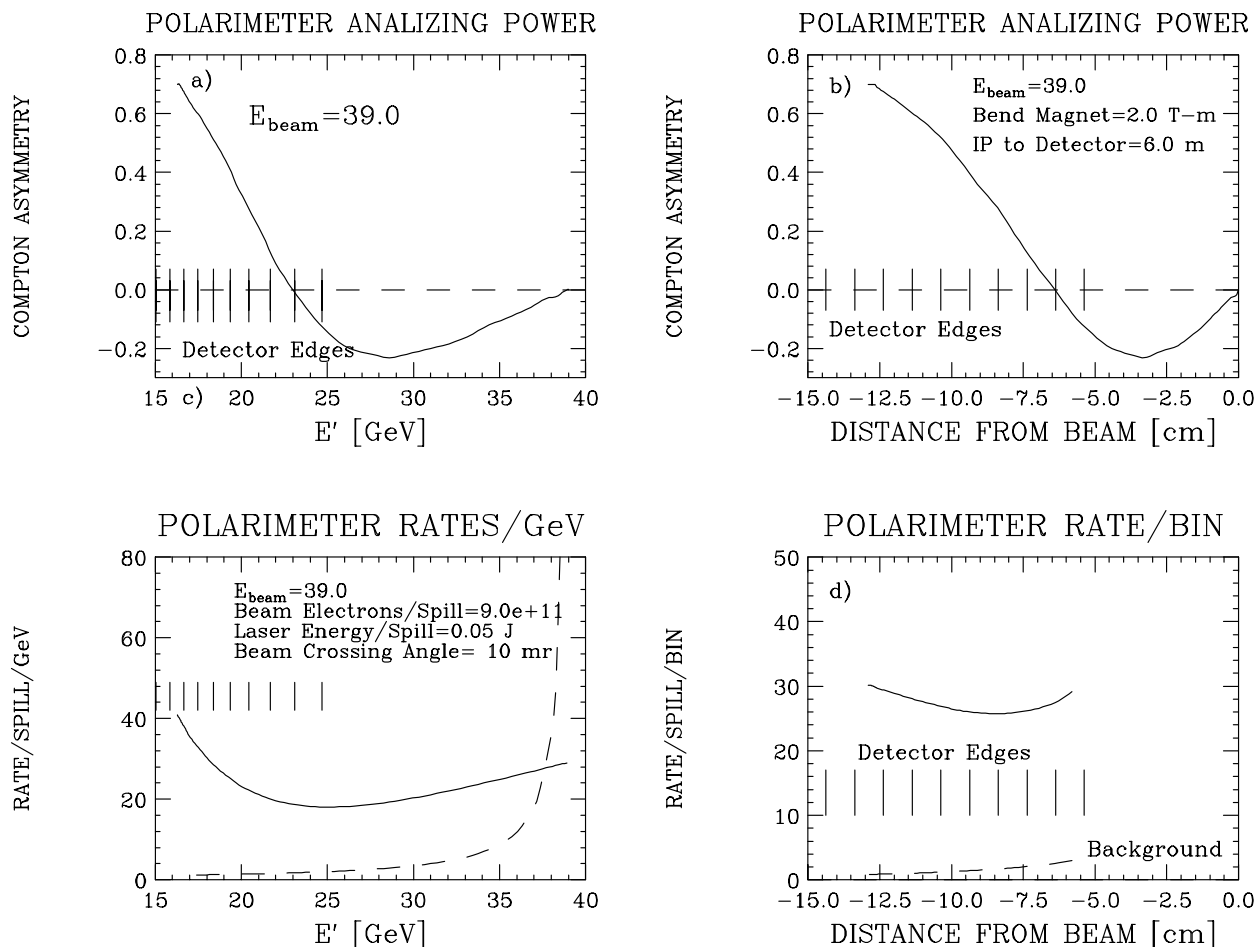


Figure 12: a) Compton asymmetry vs. scattered electron energy, b) Compton asymmetry vs. position at detector. c) Compton rate/GeV/spill vs. scattered electron energy (solid). Also shown is the estimated rate from beam gas bremsstrahlung. d) Compton rate/detector channel/spill vs. position at detector. In all plots, the edges of the SLD detector are shown as vertical lines. The laser characteristics are described in the text.

Laser and Optics

The laser used in the SLD Polarimeter was a frequency-doubled Nd:Yag laser (Spectra Physics GCR-130). Two of these lasers are available, but have not been used for 5 years and will either need to be refurbished or replaced. All of the other optics systems in the SLD polarimeter are in good shape and are available for this experiment. However, two

CCD cameras and laser beam profile systems will need to be acquired. The laser produced 6-ns pulses at 17 Hz. with beam quality sufficient to focus onto a sub-mm radius electron beam. The output wavelength is 1064 nm. After frequency doubling, the wavelength is 532 nm. The operational power at the Compton IP was 0.05 Joule/pulse (1.4×10^{17} photons/pulse). The short pulse is an advantage for background rejection since we can use timing to separate Compton events from background events due to beam gas interactions. Background in the detector is dominated by bremsstrahlung scattering of the electrons from the residual gas ($\sim 1. \times 10^{-6}$ torr) between the A-line bend and the chicane. In Fig. 12c we show the expected number of counts (per pulse per GeV) due to Compton scattering and background for a 400-ns long, 39 GeV electron pulse and 6-ns laser pulse. The laser pulse can also be moved in time relative to the start of the electron pulse. This can provide useful information on the change of electron polarization or background during the pulse. The steering can also be changed to sample different transverse parts of the beam. During SLD running, the laser fired every 7th electron pulse. Every 7 seconds the laser fired on the 6th pulse to avoid any synchronization of the laser firing with instabilities in the electron beam. Gating the electronics during the pulses when the laser is off, gives a very high statistics continuous measurement of the beam-related backgrounds.

The optical system will be the one used in SLD [52]. The photons are circularly polarized with a linear polarizer and two Pockels cells (CP and PS). The circular polarization is given by $P_\gamma = \sin(\delta_{CP}) \cos(\delta_{PS})$, where δ_{CP} and δ_{PS} are the polarization phase shifts imparted by the Pockels cells. A harmonic beam sampler before the IP transmits 98% of the laser power and generates two 1% beams which are used to measure the intensity and polarization (P_γ). Transport optics between the polarization Pockels cells and the Compton IP can change the laser beam's polarization from circular to elliptical. However, this can be compensated by adjusting δ_{CP} and δ_{PS} . Routine scans of the Pockels cells phase shifts to maximize the measured Compton asymmetry will be employed to maintain $P_\gamma = 99.9\%$ at the Compton IP. Similar scans were employed for the SLD experiment, where $P_\gamma = 99.9 \pm 0.1\%$ at the Compton IP was achieved.[53] We also plan to measure the laser polarization after the IP, as was done in SLD, to ensure that the laser beam is still fully polarized.

Chicane

The chicane consists of three 18D72 magnets separated by 8.5 m. The first and last magnets run at 2 T-m, while the middle one has exactly twice the bending power, namely 4 T-m. The first magnet bends a 39 GeV beam by 15.4 mr. We will place the SLD detector 6 m from the center of the first magnet. As shown in Fig. 12b, the detector will be 5 cm from the beamline (as in SLD) and have the Compton edge in the middle of the next-to-last detector channel. The detector is on a remote-controlled stage and can be translated to precisely locate the Compton edge.

The 16.3 to 28 GeV Compton electrons are bent by 36.8 to 21.0 mr. For a detector placed 6 m from the center of the first large chicane magnet, the corresponding dispersion varies from 1.4 to 0.6 cm/GeV, which is very similar to the dispersion in the SLD Compton polarimeter (where the bending magnet is stronger, but the drift distance shorter). The detector has 9 1-cm square cells. The 5 cm distance to the primary beam allows enough room for a vacuum window to separate the primary and scattered electrons just upstream

of the detector. The second and third large chicane magnets are necessary to restore the beam polarization to the longitudinal direction, and to point it towards Beam Dump East. We have chosen a horizontal rather than vertical deflection in order to simplify the earthquaking requirements. We used a similar chicane system in Experiments E143 and E155 to compensate for the field in the target magnet.

Detector

We will reuse SLD's segmented atmospheric pressure threshold Čerenkov detector. A remotely-insertable thin sheet of lead in front of the detector enhances the signal from high energy electrons by about a factor of five. The detector has nine 1-cm cells with about 1 GeV resolution in the bend plane and will be operated in the flux counting mode. The detector has nine phototubes, which are read out by a LeCroy 2249W ADC (though we may switch to the integrating 16-bit ADC developed for the E-158 experiment). Calibration of the detector's analyzing power is achieved with position scans, from studies of the Compton rates and asymmetries in each channel versus detector position.[54] Position scans are expected to be done every few days. Between scans, the ratios of rates and asymmetries of channels near the Compton edge can be used to monitor changes in the channel analyzing powers. The linearity of the detector is studied by comparing detector signal fluctuations with fluctuations in the electron beam and laser intensities and from scans of the laser intensity. We will also investigate improving the linearity and linearity diagnostics with the addition of an LED pulser system.

Rates and systematics

In Fig. 12 we show the results of calculations for incident electron energies of 39 GeV under conditions anticipated for this experiment. In panel c.) we show the expected number of scattered and background electrons per GeV per spill as a function of E' . The background is from beam gas bremsstrahlung between the last A-line bend magnet and the analyzing magnet using a typical vacuum of 10^{-6} torr. There is a 30 ns ADC gate around the laser pulse. This background is very small in the region of interest. The positions of the nine Čerenkov cells are indicated by the gaps between the short vertical lines. The expected analyzing power as a function of scattered electron energy is shown in panel a. In panels b) and d) we show the same quantities, plotted as a function of the distance from beam pipe at the detector. The Compton edge is located in the next to last detector channel.

The major systematic uncertainties at SLD were due to detector analyzing power calibration, detector linearity and laser polarization. Just as at SLC, we plan to spend sufficient time studying these properties to reduce the effects. The superb stability of the beam in ESA, a product of the work for E158, will make these studies easier than at SLD. We expect to exceed the SLD performance of 0.5% systematic error on the beam polarization. We will be attempting to achieve the 0.25% error desired for a future Linear Collider (LC).[55] In this regard, the ESA beam and this proposed experiment offer an excellent test beam for demonstrating some of the beam diagnostics required at the LC. In addition to the precise polarimetry desired for the LC, there is a need to demonstrate precise beam energy measurements at the level of 50-100 ppm. While this level of precision is not needed for this experiment, we note that the A-Line and ESA provide a test facility for demonstrating

precise beam energy measurements. The 180-degree spin precession of the polarized beam every 3.2 GeV can be used to calibrate and cross check an energy spectrometer. In addition, the LC beam diagnostics are required to work in the presence of significant beamsstrahlung background. Beam diagnostics downstream of the thick target employed by this experiment could be tested, using bremsstrahlung to mimic the beamsstrahlung background.

Photon Measurement Cross Check

The primary Compton polarization measurement will come from analyzing the Compton-scattered electrons. We plan to measure the asymmetry of the Compton-scattered photons as well and use this as a systematic cross check, as was done for the SLD polarimeter. This detector will be located in the middle of the chicane in the neutral beamline. It will be outside the beamline vacuum adjacent to the beam pipe and downstream of a thin exit window. We are considering two detectors: i) a threshold gas Cherenkov counter with insertable (1-2") lead pre-radiator and ii) a quartz-based calorimeter. The power asymmetry of the Compton photons has an analyzing power of 18.6%. Backgrounds in these detectors are dominated by synchrotron radiation (SR) from the upstream bend magnets. We have chosen to place a soft (1-mrad) bend magnet as the first magnet in the chicane so the SR from the hard bend chicane magnets does not hit these detectors.

We will also investigate if the electron and photon detectors can operate in a counting mode (as opposed to the primary integrating mode) as an additional cross check. This may be done in a separate T-xxx experiment, since a couple of days of running in this mode would be required to cross check the primary measurement with a precision of 0.2%.

References

- [1] A. Argento *et al.*, Phys. Lett. 140B (1984) 142.
- [2] C.Y. Prescott *et al.*, Phys. Lett. 77B, 347 (1978); 84B, 524 (1979).
- [3] Particle Data Group, Phys. Rev. D 66, (2002) 010001.
- [4] M. Chanowitz, Phys. Rev. Lett. 87 (2001) 231802, and Phys. Rev. D66 (2002) 073002.
- [5] The LEP Collaborations: ALEPH Collaboration, DELPHI Collaboration, L3 Collaboration, OPAL Collaboration, the LEP Electroweak Working Group, and the SLD Heavy Flavour Working Group, hep-ex/0212036 (2002).
- [6] NuTeV Collaboration, G.P. Zeller *et al.*, Phys. Rev. Lett. 88 (2002) 091802. Minor revisions in hep-ex/0110059 v.3 (2003) and hep-ex/0203004 v.3 (2003).
- [7] S. Davidson, hep-ph/0209316 (2002); W. Loinaz *et al.*, hep-ph/0210193 v.3 (2003).
- [8] G.A. Miller and A.W. Thomas, hep/ex-0204007 (April 2002); S.A. Kulagin, hep-ph/0301045 (January, 2003); J.T. Londergan, A.W. Thomas, hep-ph/0303155 (March 2003); NuTeV Collaboration hep/ex-0207052 (September 2002).

- [9] A.I.Milstein, O.P.Sushkov, I.S.Terekhov, hep-ph/0212072 (2002); Phys. Rev. Lett. 89 (2002) 283003; V.A. Dzuba, V.V. Flambaum, J.S.M. Ginges, Phys. Rev. D66 (2002) 076013; C.S. Wood *et al.*, Can. J. Phys. 77 (1999) 7.
- [10] SLAC-Experiment E158, E. Hughes, K. Kumar, P. Souder, spokespersons (1997).
- [11] J. Erler, A. Kurylov, M.J. Ramsey-Musolf, hep-ph/0302149 (2003) and J. Erler, private communication.
- [12] Jefferson Lab Experiment E02-020, R. Carlini, J.M. Finn, S. Kowalski, S. Page, spokespersons (2002).
- [13] R. Cahn and F. Gilman, Phys. Rev. D17, 1313 (1978).
- [14] J. Blumlein *et al.*, HERA Workshop Vol. 1, p. 69, Hamburg 1989.
- [15] J. Erler and P. Langacker, Particle Data Group, Phys. Rev. D 66, (2002) 010001.
- [16] K. Cheung, Phys. Lett. B517 (2001) 167.
- [17] P. Langacker, M. Luo, and A. Mann, Rev. Mod. Phys. 64, 87-192 (1992); P. Langacker and M. Luo, Phys. Rev. D45, 278 (1992).
- [18] M.J. Ramsey-Musolf, Phys. Rev. C60, (1999) 015501. Two corrections to this paper affecting the new physics sensitivity of DIS-PV have been found. Multiply the RHS of Eq. 45 by 8, and Eq. 46 by 1/2. The scale factor f_i for δ_1 is then 0.36 (private communication).
- [19] K. S. Babu and C. Kolda, "Z' searches", in Particle Data Group, Ref. [3], (2002)
- [20] M. Luo, numerical values for DIS parity sensitivity to $[2C_{1u} - C_{1d}]$ and $[2C_{2u} - C_{2d}]$ from Ref. [17], private communication (1992).
- [21] P. B. Straub, hep-ex/0212023 (2002).
- [22] M. Swartz, hep-ex/9912026; M. Woods, SLAC-PUB-7319; B. Schumm and R. Elia, SLD Note 222 (1992); The SLD Collaboration, SLAC-PUB-6027; M. Fero, private communication.
- [23] L. Andivahis *et al.*, SLAC-PUB-5753 (February 1992).
- [24] Y.S. Tsai, Report No. SLAC-PUB-848, 1971; Rev. Mod. Phys. 46 (1974) 815.
- [25] D.Y. Bardin *et al.*, Yad. Phys. 29 (1979) 499; Nucl. Phys. B 197 (1982) 1.
- [26] D. Relyea, E158-TN-35 (2003).
- [27] D.E. Wisner, Ph.D thesis, U. Wisconsin, 1977 (unpublished).
- [28] S-P. Li, E.M. Henley and W-Y.P. Hwang, Annals of Physics 143 (1982).

- [29] S.L. Zhu, C.M. Maekawa, B.R. Holstein and M.J. Ramsey-Musolf, Phys. Rev. Lett. 87 (2001) 201802.
- [30] T. Sjostrand, Computer Physics Commun. 82, 74 (1994).
- [31] M. Woods *et al.*, E158 TN-40.
- [32] M. Woodley *et al.*, SLAC-PUB-9233 (September 2002).
- [33] P. Castorina and P.J. Mulders, Phys. Rev. D31 (1985) 2760.
- [34] M. Osipenko *et al.*, hep-ph/0301204 (2003).
- [35] W.J. Marciano and A. Sirlin, Phys. Rev D29, 75 (1984).
- [36] Private Communication: Jens Erler.
- [37] Private Communication: William Marciano.
- [38] Private Communication: Michael J. Ramsey-Musolf.
- [39] H. Plochow-Besch/CERN-ETT/TT W5051 PDFLIB 2000.04.17.
- [40] MRST Collaboration: A.D. Martin, R.G. Roberts, W.J. Stirling, and R.S. Thorne, hep-ph/0211080 (2002).
- [41] CTEQ Collaboration: J. Pumplin, D.R. Stump, J. Huston, H.L. Lai, P. Nadolsky, and W.K. Tung, hep-ph/0201195 (2002).
- [42] S.I. Alekhin, Phys. Rev. D63 (2001) 094022.
- [43] V. Barone, C. Pascaud and F. Zomer, hep-ph/0004268 (2000).
- [44] W. Melnitchouk and A.W. Thomas, Phys. Lett. B377 (1996) 11. L.L. Frankfurt and M.I. Strikman, Nucl. Phys. B250 (1985) 1585; Phys. Rep. 160 (1988) 235.
- [45] E.N. Rodionov, A.W. Thomas and J.T. Londergan, Mod. Phys. Lett. A9 (1994) 1799.
- [46] J.T. Londergan and A.W. Thomas, hep-ph/0301147 (2003).
- [47] E. Sather, Phys. Lett. B274 (1992) 433.
- [48] Fu-Guang Cao and A. I. Signal, Phys. Rev. C62 (2000) 015203.
- [49] K. Abe *et al.*, Phys. Lett. B452 (1999) 194.
- [50] M.L. Swartz, Phys. Rev. D 58 (1998) 014010; hep-ph/9711447 (1997).
- [51] C.Y. Prescott, SLAC-TN-73-1; F.W. Lipps and H.A. Toelhoeck, Physica 20, 82 (1954). (In Eq.'s 2 and 7, p. 397, the factor $k \cos(\theta)$ should be $k_0 \cos(\theta)$).

- [52] M. Woods, SLAC-PUB-7319.
- [53] J.P. Fernandez, SLD-Note-265 (1999).
- [54] M. Fero et al., SLD Physics Note 50 (1996).
- [55] P.C. Rowson and M. Woods, SLAC-PUB-8745 (2000).